Journal of Neuroscience Methods 398 (2023) 109958

Contents lists available at ScienceDirect

Journal of Neuroscience Methods

journal homepage: www.elsevier.com/locate/jneumeth

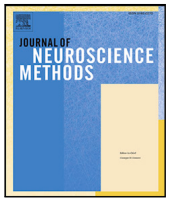

Method for quantifying arousal and consciousness in healthy states and severe brain injury via EEG-based measures of corticothalamic physiology

S. Assadzadeh [a,b,1], J. Annen [c,d,1], L. Sanz [c,d], A. Barra [c,d], E. Bonin [c,d], A. Thibaut [c,d], M. Boly [e,f], S. Laureys [c,d,g,h], O. Gosseries [c,d,2], P.A. Robinson [a,b,*,2]

[a] School of Physics, The University of Sydney, NSW 2006, Australia
[b] Center for Integrative Brain Function, The University of Sydney, NSW 2006, Australia
[c] Coma Science Group, GIGA-Consciousness, University of Liège, Belgium
[d] Centre du Cerveau, University Hospital of Liège, Belgium
[e] Department of Psychiatry, University of Wisconsin-Madison, Madison, WI, USA
[f] Department of Neurology, School of Medicine and Public Health, University of Wisconsin, Madison, WI, USA
[g] Joint International Research Unit on Consciousness, CERVO Brain Research Centre, U Laval, Canada
[h] International Consciousness Science Institute, Hangzhou Normal University, Hangzhou, China

ARTICLE INFO

Keywords:
Arousal state
Consciousness
Modeling
Electroencephalography
Classification

ABSTRACT

Background: Characterization of normal arousal states has been achieved by fitting predictions of corticothalamic neural field theory (NFT) to electroencephalographic (EEG) spectra to yield relevant physiological parameters.
New Method: A prior fitting method is extended to distinguish conscious and unconscious states in healthy and brain injured subjects by identifying additional parameters and clusters in parameter space.
Results: Fits of NFT predictions to EEG spectra are used to estimate neurophysiological parameters in healthy and brain injured subjects. Spectra are used from healthy subjects in wake and sleep and from patients with unresponsive wakefulness syndrome, in a minimally conscious state (MCS), and emerged from MCS. Subjects cluster into three groups in parameter space: conscious healthy (wake and REM), sleep, and brain injured. These are distinguished by the difference $X-Y$ between corticocortical (X) and corticothalamic (Y) feedbacks, and by mean neural response rates α and β to incoming spikes. $X-Y$ tracks consciousness in healthy individuals, with smaller values in wake/REM than sleep, but cannot distinguish between brain injuries. Parameters α and β differentiate deep sleep from wake/REM and brain injury.
Comparison with existing methods: Other methods typically rely on laborious clinical assessment, manual EEG scoring, or evaluation of measures like Φ from integrated information theory, for which no efficient method exists. In contrast, the present method can be automated on a personal computer.
Conclusion: The method provides a means to quantify consciousness and arousal in healthy and brain injured subjects, but does not distinguish subtypes of brain injury.

1. Introduction

One operational definition of consciousness is the presence of subjective experiences (Edelman, 2003; Metzinger, 1995, 2000). Consciousness is present during wakefulness and dreaming, and is also experienced by patients suffering from the "locked-in syndrome", ones who are in a minimally conscious state (MCS) (Laureys et al., 2004, 2009), or those who have emerged from MCS (EMCS). Consciousness subsides in dream-free sleep states and is restored on waking. However, the appearance of wakefulness does not always guarantee a conscious experience; a subject can demonstrate opening of the eyes, but completely lack cognitive function, such as in the "unresponsive wakefulness syndrome" (UWS), also referred to as the vegetative state (Laureys et al., 2004, 2009, 2010; Bruno et al., 2011; Gosseries et al., 2011a). In MCS, patients have partial preservation of conscious awareness (Laureys et al., 2004; Bruno et al., 2011). Patients emerged from the MCS (EMCS) recover functional communication or object use (Giacino et al., 2004). In reality, there exists a spectrum of arousal

* Corresponding author at: School of Physics, The University of Sydney, NSW 2006, Australia.
E-mail address: peter.robinson@sydney.edu.au (P.A. Robinson).
[1] Contributed equally.
[2] Contributed equally.

https://doi.org/10.1016/j.jneumeth.2023.109958
Received 24 May 2023; Received in revised form 9 August 2023; Accepted 27 August 2023
Available online 1 September 2023

and awareness, where the two are not necessarily correlated. It is thus important not only for diagnostic purposes, but also for gauging the effectiveness of anesthesia during surgery, to reliably measure the level of consciousness independent of a subject's arousal level and responsiveness (Mashour et al., 2012; Sanders et al., 2012).

The Integrated Information Theory (IIT) (Koch et al., 2016; Tononi et al., 2016), the Global Neuronal Workspace Theory (Baars, 2002; Dehaene et al., 2003), and cognitive binding (Revonsuo and Newman, 1999), are attempts at characterizing the neural basis of consciousness. IIT proposes a quantitative measure, denoted Φ, of the amount of integrated information in a physical system, which is postulated to be closely correlated with consciousness (Tononi, 2008, 2012; Oizumi et al., 2014). However, it has been argued that given the richness of conscious experience, any theory that quantifies the level of consciousness with a single measure is likely to be overly simplified and, as a result, limited in its scope (Seth et al., 2006, 2008; Freeman, 2007). Instead it has been suggested that multiple quantitative measures would more appropriately characterize the relevant complexity of the neural systems underlying consciousness (Seth et al., 2006, 2008; Freeman, 2007).

To achieve practical relevance for studying the human brain, measures of consciousness must be calculable from experimental recordings. Signal analysis methods are commonly applied to the electroencephalogram (EEG) to compute complexity measures that correlate with levels of consciousness (Kim et al., 2018; Gosseries et al., 2011b; Nunez and Srinivasan, 2006). Examples include the perturbational complexity index (PCI), a measure of the algorithmic complexity of cortical EEG in response to a strong localized stimulus delivered by transcranial magnetic stimulation (TMS) (Casali et al., 2013; Casarotto et al., 2016; Bodart et al., 2017), and the bispectral index, which is used to monitor depth of anesthesia during surgery (Gan et al., 1997; Myles et al., 2004). The main shortcoming of purely signal analysis methods is that they do not take into account the brain physiology and anatomy that actually underlie states of consciousness and generate observed EEG signals.

Supported by significant evidence of altered consciousness stemming primarily from human lesion and neuroimaging studies, corticothalamic network function is understood to be essential for consciousness (Sanders et al., 2012; Laureys et al., 2009; Laureys and Schiff, 2012), although other structures, such as the basal forebrain, are also indispensible for wakefulness (Fuller et al., 2011). In particular, breakdown of functional connectivity in the corticothalamic system has been associated with diminished levels of consciousness, including in sleep, deep anesthesia, and patients with UWS (Tononi et al., 2016; Laureys et al., 2009; Guldenmund et al., 2017; Boveroux et al., 2010). When estimated indirectly by signal analysis methods, it is found that the amount of integrated information is also noticeably reduced in these states (Casali et al., 2013; Kim et al., 2018).

Physiologically based models of brain activity have been developed using neural field theory (NFT), which averages over microscale neural properties to predict activity at scales of a few tenths of a millimeter and above (Deco et al., 2008). NFT of the corticothalamic (CT) system has been used to predict EEG spectra, with the results extensively verified against experiment (Robinson et al., 2001, 2002, 2004; Robinson, 2005; Rowe et al., 2004; van Albada et al., 2010). It has also been used to investigate the alpha rhythm (O'Connor and Robinson, 2004; Robinson, 2003), age-related changes to the physiology of the brain (van Albada et al., 2010), evoked response potentials (Rennie et al., 2002; Zobaer et al., 2018), neuroplasticity (Robinson, 2011; Assadzadeh and Robinson, 2018), and many other phenomena. The model accurately predicts EEG activity from physiologically-based parameters that correspond to experimentally measurable quantities in the brain, including parameters of the CT system across wake, REM, and NREM sleep. Conversely, its predictions can be fitted to experimental EEG spectra to estimate physiological parameters and track brain state (Abeysuriya et al., 2015; Abeysuriya and Robinson, 2016; Robinson, 2003, 2005; Rowe et al., 2004; van Albada et al., 2010); these estimates are consistent with a range of experimental EEG-related phenomena and independent physiological estimates (Robinson et al., 2004; Rowe et al., 2004). A key advantage of model-based classification is that, unlike blind signal analysis or statistical classifiers, the model parameters relate explicitly to the properties of the physical system that produces the signals.

In this work we develop a method to classify consciousness states by fitting the predictions of the above established corticothalamic model to data from EEG recordings from healthy controls, and subjects with severe brain injury, including UWS, MCS, and EMCS. These fits allow us to estimate parameters of the CT system of each subject. We use these estimates together with fits to healthy subjects' sleep and wake EEGs in order to extend previous analyses of arousal states to identify potential measures of consciousness derived from the fitted model parameters that are closely linked to corticothalamic dynamics. We then test how well these measures enable us to generalize our methods to distinguish different states of consciousness in healthy subjects and those with impaired consciousness. This study is designed to identify both robust measures and other promising ones that can later be further verified when additional brain injured subjects' data become available.

The structure of the paper is as follows: In the Theory and Methods section we present the mathematical framework of neural field theory (NFT), the corticothalamic model, and the methods used to estimate parameters. In the Results section we show that specific quantities derived from the model parameters can differentiate consciousness or its lack thereof in healthy individuals between wake/REM and NREM sleep, and distinguish healthy controls (across both wake and sleep) from brain patients with severe brain injury. The Discussion and Conclusions section summarizes and discusses the main outcomes of the work, along with future directions.

2. Theory and methods

In this section we briefly review neural field theory (NFT), the corticothalamic (CT) system, prediction of resulting EEG activity, and the algorithm used to fit the model to EEG data (Robinson et al., 1998, 2002, 2004; Rennie et al., 2002; Rowe et al., 2004; Abeysuriya and Robinson, 2016; Deco et al., 2008; Roberts and Robinson, 2012). Because these methods are unfamiliar to many researchers, sufficient detail is given to make the material reasonably self-contained.

2.1. Neural field model

The brain contains multiple distinguishable populations of neurons, which are labeled in the present work by a subscript a that designates the structure in which the population lies and/or the neurotransmitter it expresses. Neural properties are averaged over scales of ~ 0.1 mm, resulting in mean-field quantities that obey NFT equations.

At a position $\mathbf{r}$ and time t inputs from afferent neuronal populations b drive synaptic dynamics in neurons a that cause postsynaptic potential changes. These changes propagate through dendrites to the soma, causing changes in the mean soma potential $V_a(\mathbf{r},t)$ of neurons a, measured relative to resting, which approximately obey the equation (Rennie et al., 2002)

$$D_{\alpha\beta}V_a(\mathbf{r},t) = \sum_b \nu_{ab}\phi_b(\mathbf{r},t-\tau_{ab}), \tag{1}$$

where $D_{\alpha\beta}$ is defined by

$$D_{\alpha\beta} = \frac{1}{\alpha\beta}\frac{d^2}{dt^2} + \left(\frac{1}{\alpha}+\frac{1}{\beta}\right)\frac{d}{dt} + 1, \tag{2}$$

where $1/\beta$ and $1/\alpha$ are characteristic rise and decay times of the potential due to an impulse at a synapse and $\beta \geq \alpha$. The right of Eq. (1) describes the influence of the pulse rates ϕ_b arriving at population a from neuronal populations b, in general delayed by a time τ_{ab} when there are discrete anatomical separations between different structures.

The average connection strength of synapses to population a from population b is $\nu_{ab} = N_{ab}s_{ab}$, where s_{ab} is the time-integrated response in neurons of type a to a unit signal from neurons of type b (negative for inhibitory synapses) and N_{ab} is the mean number of synapses (Rennie et al., 2002; Robinson et al., 2002, 2004).

According to Eqs. (1) and (2), the response at the cell body at time t to a delta-function input to the dendrites at time t' is (Robinson et al., 2002)

$$L(u) = \frac{\alpha\beta}{\beta - \alpha}\left(e^{-\alpha u} - e^{-\beta u}\right), \tag{3}$$

where $u = t - t'$. This form is the integral kernel that corresponds to the differential operator in Eq. (2) and is a good approximation to the soma response seen experimentally; it summarizes the combined timescales of synaptic dynamics, dendritic propagation, and soma charging/discharging (Robinson et al., 1998, 2001, 2002, 2004; Rennie et al., 2002).

Action potentials are produced when the soma potential V_a exceeds a threshold θ, with a rate Q_a that rises steeply with V_a before leveling off. In a population, this dependence is smeared out by differences in individual neurons and their environments to yield the average response function (Freeman, 1975; Robinson et al., 1998, 2002, 2004)

$$Q_a(\mathbf{r}, t) = S\left[V_a(\mathbf{r}, t)\right], \tag{4}$$

where S is a sigmoid function that increases from 0 to $Q_{\max}$ as V_a increases from $-\infty$ to $+\infty$. We approximate this function by

$$S\left[V_a(\mathbf{r}, t)\right] = \frac{Q_{\max}}{1 + \exp\left\{-\left[V_a(\mathbf{r}, t) - \theta\right]/\sigma'\right\}}, \tag{5}$$

where we assume a common mean neural firing threshold θ relative to resting, with $\sigma'\pi/\sqrt{3}$ being its standard deviation (Robinson et al., 2002, 2004; Rowe et al., 2004).

Each neuronal population a produces a field ϕ_a of pulses, that travels to other neuronal populations at a velocity v_a through axons with a characteristic range r_a. This spreading activity dissipates if not regenerated and approximately obeys the damped wave equation (Jirsa and Haken, 1996; Robinson et al., 1998, 2002, 2004; Rowe et al., 2004)

$$D_a\phi_a(\mathbf{r}, t) = Q_a(\mathbf{r}, t), \tag{6}$$

$$D_a = \frac{1}{\gamma_a^2}\frac{\partial^2}{\partial t^2} + \frac{2}{\gamma_a}\frac{\partial}{\partial t} + 1 - r_a^2\nabla^2, \tag{7}$$

where the damping coefficient is $\gamma_a = v_a/r_a$. Eqs. (1)–(7) form a closed nonlinear set, which can be solved numerically or examined analytically in the linear limit (Rennie et al., 2002; Rowe et al., 2004; Robinson et al., 1998, 2002, 2004).

Stable steady state solutions of the above equations are interpreted as representing the baseline of background brain activity (defined to exclude paroxysmal states such as seizures, but to include the baselines of states of impaired consciousness considered here). These steady states have been found to have firing rates that are in accord with experiments on normal subjects (Deco et al., 2008; Robinson et al., 2002, 2004), with time dependent brain activity arising from the perturbations. Spatially uniform steady states are obtained by setting all derivatives in Eqs. (1)–(7) to zero. Previous work has successfully modeled normal brain states as lying in the linear regime (Roberts and Robinson, 2012; O'Connor and Robinson, 2004; Robinson et al., 2002, 2004; Robinson, 2003), allowing observable quantities such as transfer functions, spectra, and correlation and coherence functions to be expressed analytically. Thus, we linearize Eq. (5) by considering only first-order perturbations and write

$$Q_a(\mathbf{r}, t) - Q_a^{(0)} \approx \rho_a\left[V_a(\mathbf{r}, t) - V_a^{(0)}\right], \tag{8}$$

where

$$\rho_a = \left.\frac{dS(V_a)}{dV_a}\right|_{V_a = V_a^{(0)}}. \tag{9}$$

From now on we consider only perturbations from steady states. Eq. (9) then yields

$$Q_a^{(1)}(\mathbf{r}, t) = \rho_a V_a^{(1)}(\mathbf{r}, t), \tag{10}$$

where $Q_a^{(1)}$ and $V_a^{(1)}$ are perturbations (Robinson et al., 2002, 2004).

The Fourier transform Eqs. (1)–(10) yields the following spectral representation of activity (Deco et al., 2008):

$$\phi_a^{(1)}(\mathbf{k}, \omega) = \sum_b L(\omega)e^{i\omega\tau_{ab}}G_{ab}\Gamma_a^{(0)}(\mathbf{k}, \omega)\phi_b^{(1)}(\mathbf{k}, \omega); \tag{11}$$

$$L(\omega) = \left(1 - \frac{i\omega}{\alpha}\right)^{-1}\left(1 - \frac{i\omega}{\beta}\right)^{-1}, \tag{12}$$

$$\Gamma_a^{(0)} = \left[\left(1 - \frac{i\omega}{\gamma_a}\right)^2 + k^2r_a^2\right]^{-1}, \tag{13}$$

where $\mathbf{k}$ and ω are the wave vector (with magnitude $k = 2\pi/\lambda$ where λ is the wavelength) and angular frequency ($\omega = 2\pi f$ where f is the frequency in Hz), respectively and $L(\omega)$ and $\Gamma_a^{(0)}$ are derived from the Fourier transforms of the differential operators defined in Eqs. (2) and (7), respectively; $L(\omega)$ embodies the low-pass filter characteristics of local dynamics (Abeysuriya et al., 2015; Kerr et al., 2008; Roberts and Robinson, 2012; Robinson et al., 2002, 2004). The gains are defined by $G_{ab} = \rho_a\nu_{ab} = \rho_a N_{ab}s_{ab}$ and denote the differential response in neurons a per unit input from neurons b.

2.2. Corticothalamic model and EEG power spectrum

The corticothalamic model used here describes the interactions of four populations: cortical excitatory (e), cortical inhibitory (i), thalamic reticular (r), and thalamic relay (s) (Rowe et al., 2004; Roberts and Robinson, 2012), whose connectivity is shown in Fig. 1. The system is driven by external stimuli ϕ_n to the thalamic relay nuclei, which project to the thalamic reticular nucleus and the cortex. The long range cortical axons connect distant regions of the cortex, while some excitatory axons connect the cortex to the thalamic populations r and s. The populations i and r are inhibitory, so r and i projections suppress activity in the relay nuclei (s) and the cortex, respectively.

Eq. (11) for the CT system gives four simultaneous equations describing the pulse rates ϕ_e, ϕ_i, ϕ_r, and ϕ_s in terms of incoming activity from other populations and the external stimulus ϕ_n. Synapses projecting to the cortex have the same chance per target neuron of terminating on an inhibitory or excitatory neuron (random connectivity) (Braitenberg and Schüz, 1998; Wright and Liley, 1996). Using this simplification (i.e., $\nu_{ib} = \nu_{eb}$), we can eliminate ϕ_i, ϕ_r, and ϕ_s to obtain the transfer function to ϕ_e, with (Robinson et al., 2002, 2004, 1998)

$$\frac{\phi_e(\mathbf{k}, \omega)}{\phi_n(\mathbf{k}, \omega)} = \frac{G_{esn}\exp(i\omega t_0/2)}{(1 - G_{srs}L^2)(1 - G_{ei}L)(k^2r_e^2 + q^2r_e^2)}, \tag{14}$$

$$q^2r_e^2 = \left(1 - \frac{i\omega}{\gamma_e}\right)^2 - \frac{1}{1 - G_{ei}L}\left\{LG_{ee} + \frac{\left[L^2G_{ese} + L^3G_{esre}\right]e^{i\omega t_0}}{1 - L^2G_{srs}}\right\}, \tag{15}$$

where $G_{esn} = G_{es}G_{sn}$ is the overall gain along the path from external inputs to the cortex, and the quantities $G_{ese} = G_{es}G_{se}$, $G_{esre} = G_{es}G_{sr}G_{re}$, and $G_{srs} = G_{sr}G_{rs}$ correspond to the overall gains for the excitatory corticothalamic, inhibitory corticothalamic, and intracorticothalamic loops, respectively. The EEG power spectrum $P(\omega)$ can then be calculated by integrating $|\phi_e(\mathbf{k}, \omega)|^2$ over $\mathbf{k}$. Because of its finite size the cortex is approximated here as a rectangular sheet and periodic boundary conditions are imposed to speed numerical computation of model spectra, but this approximation does not change the results

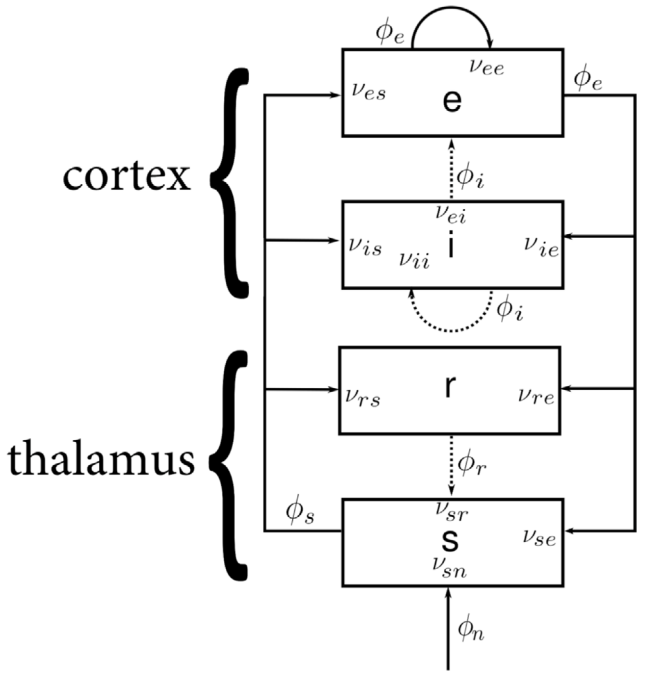

Fig. 1. Structure of the corticothalamic system. Connections are represented by arrows that show connectivity between the cortical excitatory (e) and inhibitory (i), and thalamic relay (s) and reticular (r) populations. Inhibitory connections are shown dotted (Rennie et al., 2002).

significantly (Robinson et al., 2001). This yields (Robinson et al., 2001, 2002, 2004)

$$P(\omega) = \sum_{m=-\infty}^{\infty} \sum_{n=-\infty}^{\infty} |\phi_e(k_x, k_y, \omega)|^2 F(k) \Delta k_x \Delta k_y, \tag{16}$$

$$k_x = \frac{2\pi m}{L_x}, \qquad k_y = \frac{2\pi n}{L_y}, \qquad k = \sqrt{k_x^2 + k_y^2}, \tag{17}$$

where $L_x \times L_y$ is the size of the two-dimensional rectangular cortex, with $L_x = L_y = 0.5$ m (Abeysuriya et al., 2015). The electrical activity of the cortex is spatially smoothed by volume conduction within the head when measured on the scalp, which reduces the power in spatial modes with large k. This effect is approximated by multiplying by the filter function

$$F(k) = e^{-k^2/k_0^2}, \tag{18}$$

with $k_0 \approx 10$ m^{-1} as the state-independent low-pass cutoff (Srinivasan et al., 1998; Robinson, 2003; Nunez and Srinivasan, 2006). The model power spectrum has been shown to match closely with EEG spectral data (Robinson et al., 2002; van Albada et al., 2010; Abeysuriya et al., 2015). The characteristic shape of the EEG power spectrum then depends on k_0, the temporal parameters α, β, γ, and t_0, and the gains G_{ee}, G_{ei}, G_{ese}, G_{esre}, and G_{srs}.

2.3. Stability

The stability of the CT system can be directly determined from the denominator in Eq. (14), whose zeros are the solutions of the system dispersion relation (Robinson et al., 2002; Rennie et al., 2002; Abeysuriya et al., 2015)

$$(1 - L^2 G_{srs})(1 - G_{ei} L)(k^2 r_e^2 + q^2 r_e^2) = 0. \tag{19}$$

The system is stable if all the zeros ω_0 of Eq. (20) satisfy $\mathrm{Im}(\omega_0) < 0$.

Stable brain states can be represented in a three-dimensional space, which is easier to visualize than the five-dimensional set of gains in the full linear model (Robinson et al., 2002, 2004; Roberts and Robinson, 2012; Abeysuriya et al., 2015). The reduced parameters enable simplified insights into the locations of stability boundaries, from which strengths of resonances, damping, and general features of the power spectrum can be determined. These three dimensions are defined by

$$X = \frac{G_{ee}}{1 - G_{ei}}, \tag{20}$$

$$Y = \frac{G_{ese} + G_{esre}}{(1 - G_{srs})(1 - G_{ei})}, \tag{21}$$

$$\overline{Z} = -G_{srs} = \frac{(\alpha + \beta)^2}{\alpha\beta} Z, \tag{22}$$

where the auxiliary quantity $\overline{Z}$ is introduced for brevity; X, Y, and Z parametrize corticocortical, corticothalamic, and intrathalamic loop strengths, respectively. The gains G_{ei} and G_{sr} are negative because they correspond to inhibitory connections between their respective populations, while the remaining gains are positive. The quantities X and Z are therefore positive, whereas Y can be positive or negative depending on the balance between excitatory and inhibitory corticothalamic feedback.

By substituting the parameters X, Y, and Z into Eq. (20) we find

$$0 = \left(1 - \frac{i\omega}{\gamma}\right)^2 - X - \frac{Y(1 - G_{srs})}{1 + L^2 \overline{Z}} e^{i\omega t_0}. \tag{23}$$

This equation has been widely employed to determine the locations of stability boundaries in the reduced 3D space, and provides relatively simple semiquantitative guidance and insights into low-frequency corticothalamic instabilities and the roles of feedback loops in producing them (Robinson et al., 2002; Kerr et al., 2008; Roberts and Robinson, 2012). It is strictly valid in the low-frequency limit $\omega \ll \alpha, \beta, \gamma$, but there are only moderate changes to the shape of the stability zone shown in Fig. 2 so long as $\omega \lesssim \alpha, \beta, \gamma$, a point previously discussed with regard to cortical dynamics (Robinson et al., 1998, 2002).

Only a few global instabilities occur at small ω, which can easily be visualized in XYZ space (Robinson et al., 1998, 2002; Roberts and Robinson, 2012) which highlights the roles of the three feedback loops in determining stability. To approximate the locations of stability boundaries, we first set $L = 1$ in the numerators of the terms in Eq. (24). This has the effect of enhancing the size of terms that would otherwise be more strongly low-pass-filtered; however, it makes only moderate quantitative differences to the stability zone (Roberts and Robinson, 2012; Robinson et al., 2002). However, the frequency dependence of L must be retained in the denominator $1 - L^2 G_{srs}$, which has a zero at the spindle frequency $\omega = (\alpha\beta)^{1/2}$ for $G_{srs} = -(\alpha + \beta)^2/(\alpha\beta)$ (Robinson et al., 2004, 2002; Zobaer et al., 2018). The boundaries in XYZ space of the stable zone are defined by the first instability to set in as one moves out from the origin. Analysis of stability of perturbations relative to the steady state that represents normal activity finds just four global instabilities for $k = 0$, each defining one boundary in Fig. 2 (Breakspear et al., 2006; Robinson et al., 2001, 2002, 2004). The boundary at $X + Y = 1$ is due to a slow-wave instability at $\omega = 0$, caused by the disappearance of the system's fixed point via a saddle–node bifurcation (Robinson et al., 2002; Roberts and Robinson, 2012). The right boundary is defined by an alpha instability at $\sim$ 10 Hz, via a subcritical Hopf bifurcation; the top boundary is determined by the occurrence of an intrathalamic spindle instability at $\omega = (\alpha\beta)^{1/2}$; the left boundary corresponds to an instability that sets in via a supercritical Hopf bifurcation (Breakspear et al., 2006; Robinson et al., 2002), with a theta–delta band frequency of 3 – 6 Hz toward the rear, falling toward 0 Hz at the front as the slow-wave boundary is approached (Robinson et al., 2002; Zobaer et al., 2018). These instabilities have previously been associated with pathological paroxysmal brain activity, including epileptic seizures (Robinson et al., 2002; Breakspear et al., 2006; Roberts and Robinson, 2012) but not the relatively quiescent pathological states considered here. Stable brain states must lie in the stability zone (Robinson et al., 2002; Abeysuriya et al., 2015).

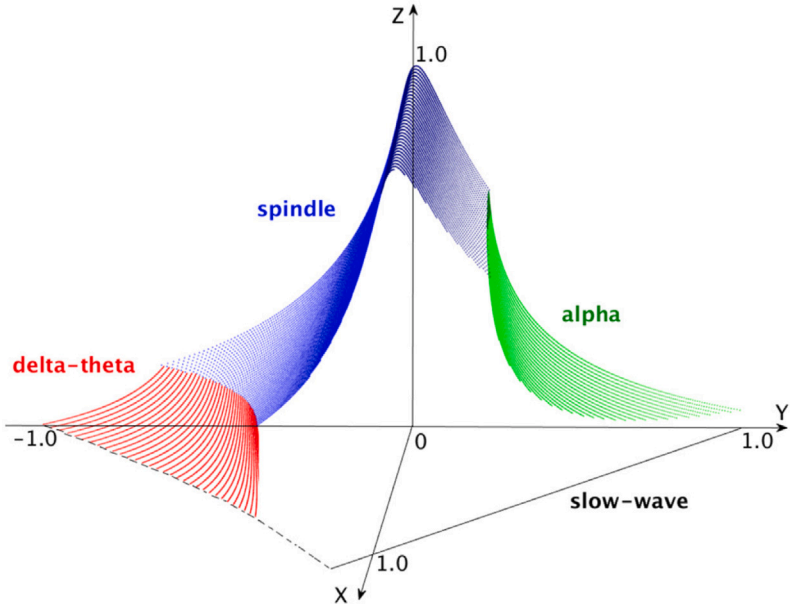

Fig. 2. Stability zone in the reduced CT model for $\alpha = 45\ s^{-1}$, $\beta = 185\ s^{-1}$, $\gamma = 116\ s^{-1}$, and $t_0 = 80$ ms. (Robinson et al., 2002; Roberts and Robinson, 2012). Colors indicate the dominant resonances close to the instability boundary, as labeled, with the front right-hand face ($X + Y = 1$ plane) left unshaded.

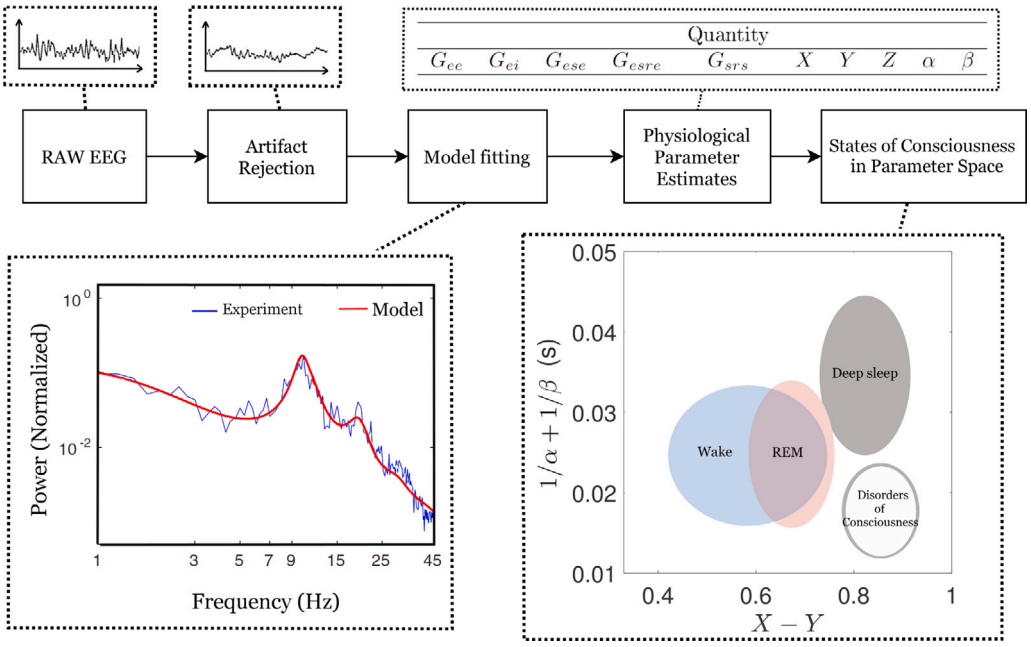

Fig. 3. Summary of the methodology and aims of the present paper. EEG artifacts are removed from raw data obtained from patients by rejecting epochs that exceed the voltage or power thresholds determined by the statistics of the data (Abeysuriya and Robinson, 2016). Corticothalamic NFT is used to predict EEG spectra, which are fitted to experimental spectra (Robinson et al., 2004; Abeysuriya et al., 2015). The fits are used to estimate neurophysiological parameters of the corticothalamic system, which are compared across states of consciousness.

2.4. Fitting and state tracking

We now briefly review the methods used to fit the model to experimental EEG data (Abeysuriya and Robinson, 2016; Robinson et al., 2004). The method uses the Metropolis–Hastings (MH) Markov chain Monte Carlo (MCMC) algorithm (Metropolis et al., 1953; Hastings, 1970). Our approach, discussed below, is summarized in Fig. 3.

Before fitting the model spectrum, we need to take into account the electromyogram (EMG) component of the experimental signals. Activity in pericranial muscles results in the EMG which increases EEG power at frequencies above $\sim$ 25 Hz. Hence, we include an EMG component $P_{\rm EMG}$ in the model power spectrum (Abeysuriya and Robinson, 2016; Rowe et al., 2004):

$$P_{\rm total}(\omega) = P(\omega) + P_{\rm EMG}(\omega), \tag{24}$$

$$P_{\rm EMG}(\omega) = A_{\rm EMG}\frac{(\omega/2\pi f_{\rm EMG})^2}{\left[1+(\omega/2\pi f_{\rm EMG})^2\right]^2}. \tag{25}$$

The units of $P(\omega)$ in Eq. (17) are s^{-1}, because $\int P(\omega)d\omega$ has the same units as $\left[\phi_e(t)\right]^2$, and $\phi_e(t)$ has units s^{-1}. Thus the units of $P_{\rm total}(\omega)$

and A_{EMG} are also s^{-1}. Because the experimental power spectrum has units V^2 s, it is obtained by multiplying $P_{\mathrm{total}}(\omega)$ by a dimensional constant (Robinson et al., 2001, 2004). Experimental ranges for A_{EMG} and f_{EMG} are listed in Table 2.

Let $\mathbf{x}_{\mathrm{opt}}$ be the vector of parameter values that yields the best match to the experimental power spectrum P^{exp}. The goodness of fit is characterized by the weighted squared fractional difference between the model prediction $P(\mathbf{x})$ and P^{exp}, written as

$$\chi^2(\mathbf{x}) = \sum_j W_j \left| \frac{P_j(\mathbf{x}) - P_j^{\mathrm{exp}}}{P_j^{\mathrm{exp}}} \right|^2, \tag{26}$$

where j labels the frequency components of the fast Fourier transform. The function $W_j \propto f_j^{-1}$ provides equal weighting for each frequency decade (Rowe et al., 2004) to compensate for the larger number of points per decade at high frequencies.

The MH algorithm is used to generate samples of a *posterior distribution* $p(\mathbf{x}|P^{\mathrm{exp}})$, which is maximal at $\mathbf{x}_{\mathrm{opt}}$ and not known in advance. We write the posterior distribution as

$$p(\mathbf{x}|P^{\mathrm{exp}}) \propto L(\mathbf{x}), \tag{27}$$

$$L(\mathbf{x}) = \exp\left[\frac{-\chi^2(\mathbf{x})}{2}\right], \tag{28}$$

where the likelihood function $L(\mathbf{x})$ is maximal when χ^2 is minimized at $\mathbf{x}_{\mathrm{opt}}$. Samples are generated using a random walk, with increments sampled from a normal distribution centered at $\mathbf{x}_i$ (proposal distribution) and the next step$\mathbf{x}_{i+1}$ is accepted with probability $p(\mathbf{x}_{i+1})/p(\mathbf{x}_i)$. The set of successively accepted $\mathbf{x}_i$ traversed by the walk defines a chain of points in parameter space, whose distribution of the parameter values converges to $p(\mathbf{x}|P^{\mathrm{exp}})$ as the chain grows longer. A total of 10^4 points are sampled by the chain with the first 10% discarded to exclude transients.

To track temporal changes in parameters, and thus the brain state, Bayes's theorem is applied, which uses the posterior distribution of each fit as the prior distribution of the next fit; i.e.,

$$p_{t+1}(\mathbf{x}) \propto L(\mathbf{x}) p_t(\mathbf{x}). \tag{29}$$

Updating the priors at successive fits reduces the sensitivity of the fits to rapid changes in the spectrum, which are more likely to be due to noise than true state changes. This also increases the efficiency of the method by narrowing down the parameter space from which the next set of parameters is sampled.

2.5. Data acquisition and preprocessing

Patients with severe brain injuries were diagnosed according to the best out of five Coma Recovery Scale-Revised (CRS-R) evaluations performed by experienced and trained clinicians (Giacino et al., 2004; Wannez et al., 2018) within one week of hospitalization. Inclusion criteria for the study consisted of confirmed diagnosis of a disorder of consciousness or being EMCS. No restrictions on etiology were present. All patients were medically stable, spontaneously breathing, residing in a hospital, rehabilitation center or at home. Patients were suffering from a prolonged brain injury (> 28 days after injury) and hospitalized for a one-week assessment of their state of consciousness by means of a multimodal assessment including behavioral and neuroimaging paradigms. Exclusion criteria consisted of large (open) cranectomies. See Table 1 for the demographic and clinical data of the patients with severe brain injury.

High-density EEG recordings (256 scalp saline-solution electrodes, Electric Geodesics) were obtained with a sampling rate of 500 Hz. Resting state EEG recordings were done in the dark for about a duration of 30–40 min. The EEG was performed about 10 min before until half hour after the F-FDG injection for a PET scan before which the sensor net was removed. Patients were continuously monitored to be awake (i.e., eyes open) and were aroused using the arousal stimulation protocol as described in the CRS-R if repeated or prolonged eye closure was observed.

Table 1
Summary of brain-injured patient demographics and average CRS-R sub-scores (Giacino et al., 2004) for the EMCS, MCS, and UWS groups. Etiology for traumatic brain injuries: 7 UWS, 26 MCS, 4 EMCS. Etiology for other categories (e.g., stroke, cardiac arrest): 9 UWS, 22 MCS, 5 EMCS. Mean time since injury (months): 31 ± 45 UWS, 39 ± 42 MCS, 32 ± 44 EMCS.

		Diagnosis		
		EMCS	MCS	UWS
N		9	48	16
Age (mean)		41	38	36
Age (range)		18–66	5–73	21–59
N male, female		6, 3	26, 22	7, 9
CRS-R subscale (Avg.)	Auditory (4)	3.4	2.6	1.3
	Visual (5)	4.1	2.8	0.7
	Motor (6)	5.3	2.8	1.8
	Oromotor (3)	2.8	1.6	1.6
	Communication (2)	1.6	0.2	0
	Arousal (3)	2.6	1.7	1.8
	Avg. Total (23)	19.8	11.6	7.1
	Med. Total	21.0	11	7
	IQR Total	6.0	5	2

The EEG data were collected from healthy awake controls (n = 30), UWS (n = 16), MCS (n = 48), and EMCS (n = 9) subjects. Patient demographics and CRS-R scores for the brain-injured subjects are listed in Table 1. Sleep data were obtained from a previous study of 28 manually scored polysomnograms (AASM protocol) of healthy controls (Abeysuriya and Robinson, 2016), recorded in two earlier clinical studies (D'Rozario et al., 2013; Wang et al., 2005), and fitted using the same model. The reader is referred to the references cited for further details.

The EEG data were imported into MATLAB (2019) for analysis. Power spectra were obtained from electrodes located on top of the scalp (47 electrodes), excluding face, neck, and ear locations. Spectra were computed within a rectangular sliding window of 4 s moved in 1 s increments. The final spectra used in the fits are generated by averaging the 4 s blocks inside a 30 s sliding window (average of 27 spectra for the 4 s intervals starting at 0, 1, 2, … 26 s within each sliding window). The purpose of using a longer window of 30 s is to further reduce noise and exclude blocks containing artifacts when calculating the average. A 4 s block is rejected for inclusion in the cumulative 30 s spectrum if any of the following occur: (i) If the power at frequencies below 4.5 Hz in the block lies outside 3 standard deviations of the mean of such powers across all 4 s windows. (ii) If the block contains high frequency artifacts. Specifically, if the power integrated from 30 to 45 Hz is more than 3 standard deviations higher than the mean in all the 4 s blocks. (iii) If the voltage does not change in an interval greater than 0.5 s, which may be due to problems with the recording device. This resulted in approximately 5% of blocks being discarded.

For each subject, an EEG of duration ~ 30 min, or ~ 1800 spectra, is analyzed and fitted, following the method outlined in Section 2.5. The theoretical EEG spectrum in Eq. (17) has 15 parameters that determine the shape of the spectrum, as listed in Table 2. These parameters have previously been estimated in normal wake states (Rowe et al., 2004; Robinson et al., 2004), across sleep stages (Abeysuriya et al., 2015), and abnormal states including seizures (Robinson et al., 2002; Zhao and Robinson, 2015) and Parkinson's disease (Müller et al., 2017; van Albada and Robinson, 2009). Explorations of variants of the model with significantly more parameters have also shown that the use of too many additional parameters leads to an increase in fit error and inability to obtain robust estimates of the parameters (Rowe et al., 2004).

The reduced CT model with the 5 gains listed in Table 2 has been found to offer the best quality and robustness of fits when compared via model selection criteria such as the Bayesian information

Table 2
Physiological estimates of parameter ranges and initial step sizes used in the MCMC random-walk. The fitted parameters are ones where the value of the initial step size is specified. The values for fixed parameters are based on previous work (Kim et al., 1997; Lopes da Silva et al., 1974; Suffczynski et al., 2001; Robinson et al., 2002, 2004; Roberts and Robinson, 2012; Rennie et al., 2002; van Albada et al., 2010; Rowe et al., 2004). The constraints on the fitted parameters are from previous works (Abeysuriya et al., 2015; Abeysuriya and Robinson, 2016).

Parameter	Description	Value	Step size	Unit
γ_e	Cortical damping rate	116	–	s^{-1}
r_e	Excitatory axon range	86	–	mm
Q_{max}	Maximum firing rate	340	–	s^{-1}
θ	Firing threshold	12.9	–	mV
σ'	Threshold spread	3.8	–	mV
L_x, L_y	Linear dimensions of cortex	0.5×0.5	–	m
ϕ_n	Input stimulus amplitude	1×10^{-5}	–	s^{-1}
G_{ee}	Excitatory cortical gain	0–20	0.4	–
$-G_{ei}$	Inhibitory cortical gain	0–40	0.4	–
G_{ese}	Corticothalamic loop gain	0–40	1	–
$-G_{esre}$	Corticothalamic loop gain	0–40	1	–
$-G_{srs}$	Intrathalamic loop gain	0–5	0.2	–
α	Decay rate of cell-body potential	10–100	5	s^{-1}
β	Rise rate of cell-body potential	100–800	40	s^{-1}
t_0	Corticothalamic loop delay	75–140	5	ms
A_{EMG}	Normalized EMG power	10^{-15}–10^{-12}	5×10^{-14}	s^{-1}
f_{EMG}	Characteristic EMG frequency	10–50	0.2	Hz

criterion (BIC), which measures the relative quality of a model based on the goodness of fit, but with a penalty on the number of model parameters (Abeysuriya and Robinson, 2016).

The cortical damping rate γ_e, excitatory axon range r_e, sigmoid voltage-firing response parameters $Q_{\max}$, θ, and σ', and the cortical dimensions L_x and L_y, are fixed here to previously determined values (Rowe et al., 2004; Abeysuriya et al., 2015). The physiological ranges for the fitted parameters are listed in Table 2, and are consistent with ranges obtained from independent experimental data and theoretical estimates (Lopes da Silva et al., 1974; Suffczynski et al., 2001; Robinson et al., 2004; Rowe et al., 2004; Abeysuriya et al., 2015).

The fits allow the compound gains in the model to be inferred: $G_{ese} = G_{es}G_{se}$ is the net gain of the direct corticothalamic feedback; $G_{esre} = G_{es}G_{sr}G_{re}$ is the net corticothalamic feedback via r (thalamic reticular nucleus); and $G_{srs} = G_{sr}G_{rs}$ is the net gain between the relay nuclei (s) and r. The reduced parameters X, Y, and Z are combinations of the gains. From these parameters the strengths of resonances, damping, and general features of the power spectrum can be determined.

2.6. Linear discriminant analysis

A linear discriminant analysis (LDA) was performed using the standard Matlab LDA routine (MATLAB, 2019) to classify the subjects into three categories, comprising healthy conscious states (wake and REM), healthy sleep (N3) states, and patients with severe brain injury (UWS and MCS). Because of the limited number of data, it was impossible to carry out cross-validation, so this classification should be considered to be provisional.

3. Results

Probability density functions (PDFs) of the fitted gain parameters in normal states (wake, REM, and NREM sleep) and UWS are shown on the left panels in Fig. 4. To avoid excessive overlap of plotted distributions, MCS and EMCS are shown in the right panels with a repeat of UWS for comparison. (i) The clearest overall difference occurs for the cortical excitatory gain G_{ee}, which is found to be larger in deep sleep (N3) and UWS, with lower values and larger variability during wake and REM sleep. (ii) The distributions of G_{ee} in brain-injured subjects strongly overlap (Fig. 4A and B) and are similar to that in deep sleep. (iii) In healthy subjects, increasing cortical excitation in sleep is accompanied by anticorrelated changes in G_{ei} that reflect a decrease in cortical inhibition. These cortical changes have previously been argued to compensate for the decrease in corticothalamic feedback G_{ese} in sleep (Abeysuriya et al., 2015). (iv) Average G_{ei} is similar across abnormal states and sleep (-18 ± 3), with less inhibition and larger standard deviations in REM (-17 ± 4), and wake (-13 ± 4). (v) The positive corticothalamic feedback G_{ese}, differentiates between wake (13 ± 7), and other states (4 ± 2), which include both REM and non-REM sleep, and patients with severe brain injury. (vi) The negative corticothalamic feedback G_{esre}, which incorporates the contribution of the inhibitory reticular nucleus of the thalamus, is anticorrelated with G_{ese}; i.e., there is more corticothalamic inhibition in wake (-7 ± 6) than in other states (-4 ± 2). (vii) The intrathalamic inhibition G_{srs} is small in brain-injured subjects (-0.1 ± 0.1), and stage 3 sleep (-0.09 ± 0.10), and relatively larger inhibition is observed in REM (-0.4 ± 0.3), and wake (-1.1 ± 0.8).

Fig. 5 shows the PDFs of X, Y, and Z from Eqs. (21)–(23). This 3D space is a useful representation of model states because stability and key spectral features chiefly depend on these quantities (Robinson et al., 2002). The intracortical loop gain X is reduced in wake and REM, and is reflected in flattening of the power spectrum below ~ 1 Hz. As shown in Fig. 5A and B, X differentiates the healthy conscious states of wake ($X = 0.7 \pm 0.1$) and REM ($X = 0.7 \pm 0.1$) from deep sleep ($X = 0.9 \pm 0.1$) and subjects with disorders of consciousness and brain injuries ($X = 0.9 \pm 0.1$). High X corresponds to the cortex being increasingly self-driven and disconnected from external inputs and feedbacks (Robinson, 2017).

The distributions of the total corticothalamic loop gain Y are shown in Fig. 5C and D. The parameter Y is anticorrelated with X, because wake states with large values of Y require small values of X for the state to be linearly stable. This relationship between X and Y is also related to the observation in both theory and experiment that the brain operates near marginal stability (i.e., criticality), and the wake states lie close to the stability boundary $X + Y = 1$ (Roberts and Robinson, 2012; Breakspear et al., 2006; Robinson et al., 2002; Stam, 2005; Robinson, 2017). In general, wake states are associated with smaller X (cortical) and larger positive Y (corticothalamic) than sleep states (Robinson et al., 2002; Abeysuriya et al., 2015). The larger values of Y in wake ($Y = 0.1 \pm 0.1$) indicate positive feedback between the cortex and the thalamus, which is also characteristic of a strong alpha peak arising from the corticothalamic loop in relaxed waking (Robinson et al., 2002). During REM ($Y = 0.03 \pm 0.09$) and light sleep stages there is relatively weak corticothalamic interaction, which suppresses the alpha peak. The statistical distributions peak at strong intracortical coupling

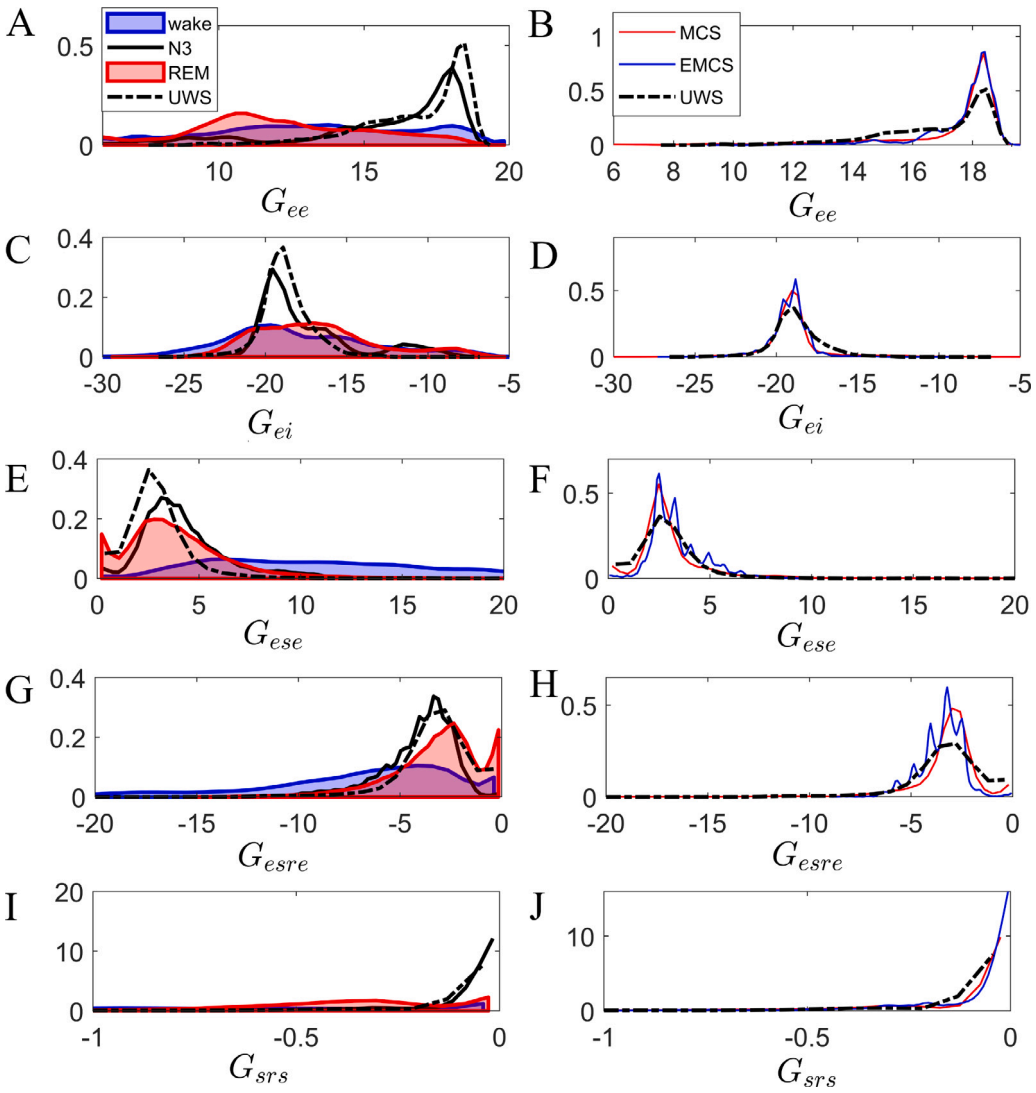

Fig. 4. Probability density functions for gains in the reduced CT model derived from fitted parameters and normalized to have the same integral. These distributions are aggregated over all the multiple fits made during the recording for each subject, and over all subjects in each group. Left column: Distributions of the indicated gains in healthy arousal states (wake, REM sleep, and deep sleep/N3), and those in unresponsive wakefulness syndrome (UWS). Right panels compare the corresponding gains in minimally conscious state (MCS), emerged from MCS (EMCS), and unresponsive wakefulness syndrome (UWS). Note that blue and red are used for different groups in the left and right columns.

(large X) and near-criticality ($X + Y \approx 1$) in deep sleep and states in brain-injured subjects, which places these states at small Y.

The intrathalamic loop gain Z has previously been shown to be large only when sleep spindles are present and can differentiate lighter sleep stages from deep sleep (Abeysuriya et al., 2015). The distributions of Z are shown in Fig. 5E and F. The average intrathalamic feedback is found to be largest in wake ($Z = 0.2 \pm 0.1$), followed by REM ($Z = 0.05 \pm 0.05$), deep sleep ($Z = 0.01 \pm 0.02$), and subjects with severe brain injury ($Z = 0.01 \pm 0.03$), all subject to $Z \geq 0$.

The distributions of α and β across healthy arousal states and injured brain states are plotted in Fig. 6. The rates α and β, are those of the fall and rise of the soma response, respectively, and together account for low-pass filtering in the model due to synaptodendritic effects. We find significantly smaller values in non-REM sleep ($\alpha = 32 \pm 10$ s^{-1}) than in wake ($\alpha = 53 \pm 20$ s^{-1}), REM ($\alpha = 52 \pm 20$ s^{-1}), and UWS ($\alpha = 52 \pm 20$ s^{-1}). In previous studies, increased sensory processing (eyes-open) relative to an absence of visual processing (eyes closed) was associated with larger α (Robinson et al., 2004; Rowe et al., 2004; Abeysuriya et al., 2015). This is consistent with the larger α observed in groups where some form of visual activation is present. Comparison of α across the disorders of consciousness (Fig. 6A and B) shows similar distributions in UWS ($\alpha = 52 \pm 20$ s^{-1}), MCS ($\alpha = 63 \pm 20$ s^{-1}), and EMCS ($\alpha = 57 \pm 10$ s^{-1}).

The parameters α and β in the model are weighted averages that capture the neurotransmitter dynamics over the corticothalamic system. Previous works have shown that α and β are correlated, with $\beta \approx 10\alpha$ (Robinson et al., 2004; Niedermeyer and Lopes da Silva, 2005). In general, the negative thalamic feedback is more dominant during sleep, which is consistent with the observation that the $GABA_B$ receptor is more active in sleep states and results in a fall of the synaptic response rates (Robinson et al., 2004). Thus wake states are typically associated with larger rates α and β than sleep states.

The distributions of β in the groups are seen in Fig. 6C and D, which show a distinction between values of β in healthy states vs. brain-injured. The distributions lean toward smaller β in wake ($\beta = 300 \pm 160$ s^{-1}), REM ($\beta = 370 \pm 160$ s^{-1}), N3 ($\beta = 320 \pm 120$ s^{-1}), and larger β in UWS ($\beta = 560 \pm 170$ s^{-1}), MCS ($\beta = 620 \pm 170$ s^{-1}) and EMCS ($\beta = 590 \pm 110$ s^{-1}). The parameter estimates from all the studied groups are summarized in Table 3.

3.1. Healthy vs. injured subjects in state space

The correlations and differences in the physiological parameters discussed in the previous section motivate us to search for parameters

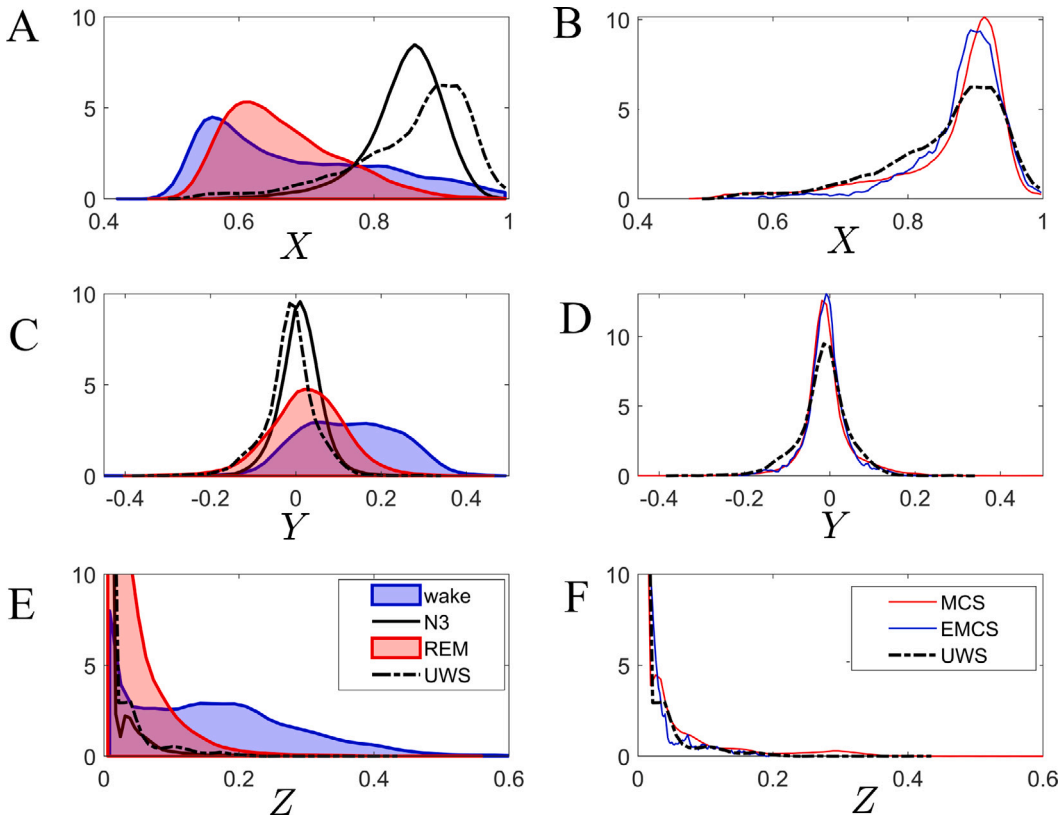

Fig. 5. Distributions of the total cortical loop gain X, total corticothalamic loop gain Y, and total intrathalamic loop gain Z in healthy arousal states and disorders of consciousness. Left column: PDFs in wake, REM sleep, deep sleep/N3 and UWS. Right column: distributions of X, Y, and Z, in UWS, MCS, and EMCS. Note that blue and red are used for different groups in the left and right columns.

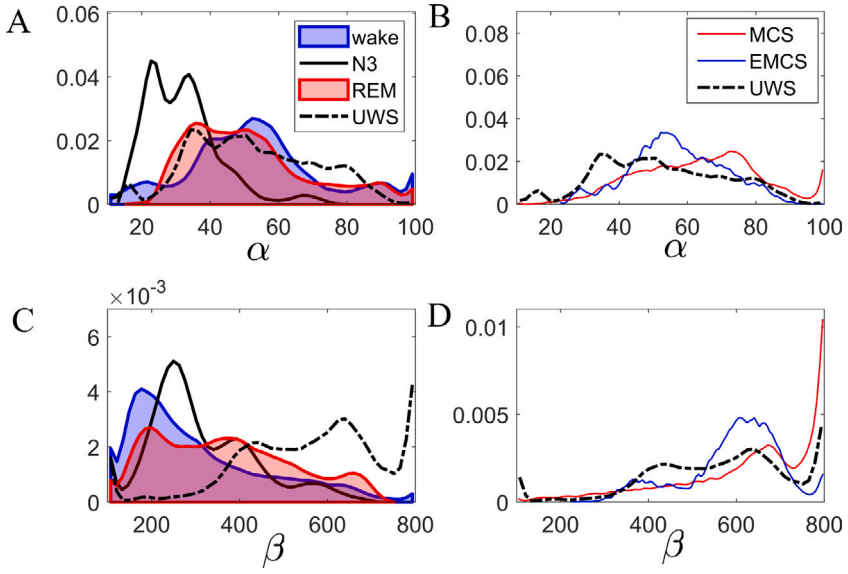

Fig. 6. Distributions of α and β, which correspond to rise and fall rates of the soma response, respectively. Left column compare the distributions of α and β in wake, REM sleep, deep sleep/N3 and UWS, while the distributions of brain-injured subjects (UWS, MCS, and EMCS) are plotted in the right column. Note that blue and red are used for different groups in the left and right columns.

that can successfully differentiate between the various brain states. The first key parameters to consider are the total intracortical (X) and corticothalamic loop gains (Y). Points in Fig. 7A represent the mean values of X and Y for $n = 134$ subjects (note that N3 sleep and REM data were collected from the same subjects), estimated from $\sim$ 30 min EEG recordings. Points in XY space reflect key features of the corresponding power spectra. Smaller X values (weak cortical feedback) and larger Y (larger corticothalamic feedback) are signatures of wake, which places wake states toward the top-left of Fig. 7 (blue circles). On the other hand, deep sleep states tend to occupy the bottom-right (black circles), while the lighter sleep states (N1, N2, and REM) are scattered in between. The mean X and Y values for UWS, MCS, and EMCS subjects are also shown for comparison. The X and Y values for the brain-injured states lie mostly toward the bottom right corner

Table 3
Mean parameters for representative examples of each brain state. Parameter values are obtained by fitting the model to EEG spectra obtained from 131 subjects (~ 1800 spectra for each subject). The fitting method is described in Abeysuriya and Robinson (2016), and is briefly reviewed in Section 2.4. Because mean values are similar in MCS and EMCS, these groups are combined for brevity in the column headed EMCS/MCS.

Quantity	$n = 30$ Wake	$n = 28$ REM	$n = 28$ N3	$n = 16$ UWS	$n = 57$ EMCS/MCS
G_{ee}	13.1	11.9	15.4	16.9	16.3
G_{ei}	−17.9	−16.9	−17.2	−18.8	−19.0
G_{ese}	12.1	3.9	4.2	3.0	3.5
G_{esre}	−7.4	−3.2	−4.0	−3.3	−3.7
G_{srs}	−1.0	−0.38	−0.09	−0.15	−0.22
X	0.69	0.67	0.84	0.86	0.87
Y	0.12	0.03	−0.01	−0.01	−0.01
Z	0.15	0.05	0.01	0.01	0.02
α	53	52	32	52	62
β	310	370	310	560	470

of the plot in Fig. 7, which places them near stage 3 non-REM (N3) sleep.

Each coarse-grained phenomenological AASM arousal stage corresponds to a range of possible spectra. For example, the alert waking state is qualitatively different from a drowsy wakeful state and the difference is readily noticed when the two spectra are compared; yet both these states are often simply classified as 'wake'. The variations within the stages can thus account for much of the apparent intersubject variability of X and Y in Fig. 7.

The dashed diagonal line $X + Y = 1$ corresponds to a saddle–node bifurcation of the model dynamics. States above this line are linearly unstable and have previously been shown to represent unstable brain dynamics such as in epileptic seizures (Roberts and Robinson, 2012; Robinson et al., 2002). The values of $X + Y$ determine the degree of criticality (Robinson et al., 2002; Robinson, 2017); for $X+Y$ just below unity, the resulting near-critical dynamics allows for complexity and information processing (Robinson et al., 2001, 2002; Robinson, 2017). The estimated states are all distributed with $0.6 \lesssim X + Y \lesssim 0.9$, and we observe that REM has lower average $X+Y$ than other states, and show greater intersubject variability.

As seen in Fig. 5, estimates of mean X and Y in patients with severe brain injury are distributed similarly to those of healthy subjects in deep sleep, where the level of consciousness is minimal. The quantity $X-Y$ is used to parametrize the level of healthy consciousness, because the largest variance occurs along the $X - Y$ axis. The dotted lines orthogonal to the stability boundary in Fig. 7A show values of $X - Y$ and demonstrate that conscious wake and sleep (REM) states can be largely differentiated from deep sleep and brain-injured patients by a partition at $X - Y \approx 0.73$.

Because of the variances along $X+Y$ and $X-Y$ in the states observed in Fig. 7A, we replot the subject means in these coordinates in Fig. 7B, showing boundaries of three regions that separate wake, REM, and deep sleep/brain injury. These simple criteria correctly classify 79% of points into REM, with a 4% false positive rate. The boundaries successfully separate 79% of wake states (8% false positive), and deep sleep and brain-injured states are distinguished from the other two groups with a success rate of 93% and false positive rate of 11%.

3.2. Synaptic response rate differences between healthy and brain-injured subjects

As shown in Fig. 5, the values of β are larger in patients with severe brain injury ($\beta \approx 650 \pm 100$ s^{-1}), than for healthy subjects in different states of arousal ($\beta \approx 300 \pm 150$ s^{-1}), whereas α is similarly distributed in both brain-injured cases and healthy conscious (wake and REM) with $\alpha \approx 50 \pm 20$ s^{-1}, but in N3 sleep the value is smaller with $\alpha \approx 30 \pm 10$ s^{-1}. As discussed in Section 2.1, α and β determine the profile of the effective soma response to an incoming spike; its the characteristic fall and rise times are $1/\alpha$ and $1/\beta$. Individual values of these response rates are shown in Fig. 8. The observed reduction of α in deep sleep (Fig. 8A), and increase of β in brain-injured subjects (Fig. 8B) relative to other groups, indicate average slower and faster synaptic responses in those states, respectively. The change in the synaptic response via these two different pathways hints at possible different mechanisms that underlie the differences in synaptodendritic dynamics in these states. Robinson et al. (2004) argued that the slower responses in deep sleep/N3 were consistent with the greater role of feedback via the reticular thalamic nucleus in this state, a nucleus in which the relatively slow $GABA_B$ dynamics is dominant.

The plot of β vs. α in all the studied groups is shown in Fig. 8D. The Pearson correlation coefficient r is highest in the brain-injured group ($r = 0.7$), followed by healthy wake and sleep ($r = 0.3$), and REM sleep ($r = 0.2$).

In order to reduce α and β to a single quantity that reflects the effective soma response time, we consider the characteristic time scale of synaptodendritic and soma-charging effects given by $t_{\alpha\beta} = 1/\alpha + 1/\beta$, which approximates the width of the response curve introduced in Eqs. (3) and (4). The mean of $t_{\alpha\beta}$ and $X - Y$ in the individuals is plotted in Fig. 8C. The horizontal axis approximately reflects the level of consciousness, with progressively larger values as we go from wake, to REM, and to deep sleep and brain-injured states. The vertical axis is the characteristic duration of the synaptic response $t_{\alpha\beta}$, and it differentiates severe brain injury from healthy sleep and wake states.

A linear discriminant analysis (LDA) was performed using the standard Matlab LDA routine (MATLAB, 2019) to classify the subjects into three categories, comprising healthy conscious states (wake and REM), healthy sleep (N3) states, and patients with severe brain injury (UWS and MCS). Because of the limited number of data, it was impossible to carry out cross-validation, so this classification should be considered to be provisional. However, as illustrated in Fig. 9, it shows that healthy conscious states are differentiated from brain injury and sleep by the approximately vertical line at $X - Y \approx 0.73$. On the other hand, the quantity $1/\alpha + 1/\beta$ separates sleep from the other two categories.

4. Discussion and conclusions

We have developed a method to classify arousal and consciousness in healthy and brain injured subjects. This involved fitting an established corticothalamic model to EEG data from subjects in various states of consciousness, including wake, REM sleep, deep sleep (N3), and severely brain-injured subjects, including patients suffering from UWS, MCS, and EMCS. Estimates of physiological parameters associated with corticothalamic dynamics were obtained from these fits of our corticothalamic neural field model to EEG spectra. The estimates were then compared to previous parameter values in sleep ($N = 28$), which allowed direct comparison of large-scale physiological parameters across various states of consciousness and arousal.

Based on the parameter differences at the group and individual level, we have found that the measure $X - Y$, which characterizes the difference of normalized strengths of corticocortical (X) and corticothalamic (Y) feedbacks, approximately tracks levels of consciousness in healthy subjects. The difference $X-Y$ is found to be sensitive to graded changes in the level of consciousness; it is minimal during normal wake and increases progressively with sleep depth and in brain-injured subjects. In healthy subjects we found a threshold value of $X-Y \approx 0.73$ above which consciousness is reduced (in NREM sleep). This parameter also separates brain-injured from healthy conscious states, but does not distinguish between brain injury subtypes (i.e., between UWS, MCS, and EMCS).

These results accord with large X and small Y indicating strong corticortical interactions with less input from thalamus and the external world. It is also consistent with fMRI studies in healthy volunteers during visual perception (Min et al., 2020) and illusions (Schmidt et al., 2020) that show that the absence of conscious perception is associated

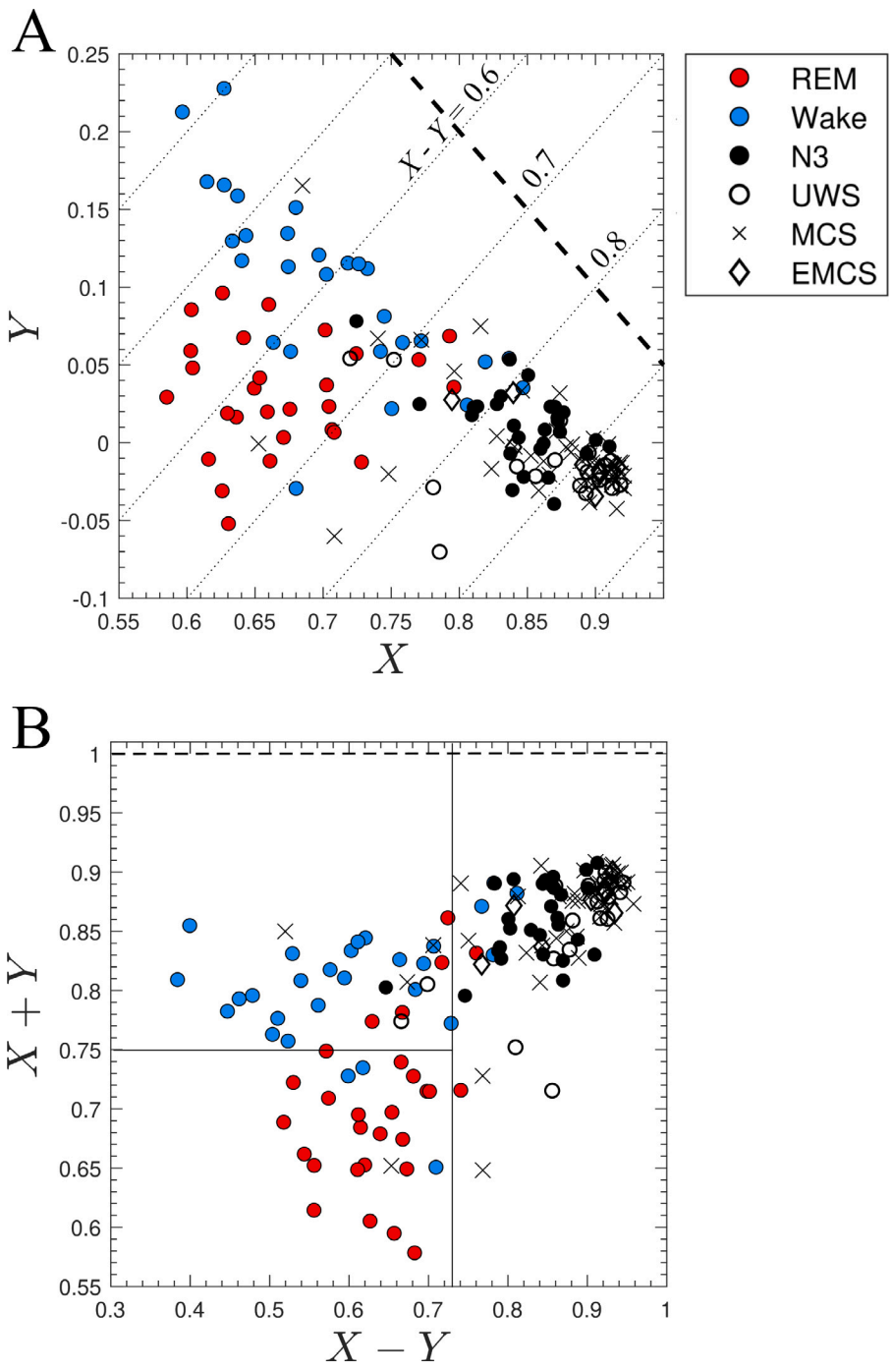

Fig. 7. (A) Mean X and Y in healthy individuals during wake, REM, and deep sleep (N3), and patients with severe brain injury. (B) Mean $X+Y$ vs. mean subject $X-Y$ for the same subjects. The filled circles mark healthy conscious subjects (blue for wake, and red for REM sleep), black circles mark healthy sleep subjects (N3), and open symbols are used to mark the brain-injured subjects. The dashed line corresponds to $X+Y=1$ and separates stable brain dynamics from unstable ones that lie above it (e.g., seizures). The orthogonal dotted lines show values of $X-Y$, as labeled.

with a decoupling of the thalamus and cortex. In patients with disorders of consciousness, (covert) fMRI task performance was positively related to corticothalamic connectivity strength, suggesting that a specific balance between corticothalamic connectivity is required for consciousness (Monti et al., 2015). Indeed, using electrophysiology it has been shown that the cortical circuits silence in patients with pathological loss of consciousness, lacking thalamic driving input (Rosanova et al., 2018). EMCS/MCS patients are considered unconscious according to the cortico-cortical and corticothalamic criteria. This is surprising, because MCS patients and especially those who show motor response to command (MCS plus) (Bruno et al., 2011) have been reported to have preserved dynamics between the thalamus and motor cortex (Fernández-Espejo et al., 2015). Our results might reveal a different pattern, as we consider the gain averaged over the whole cortex, rather than a specific cortical area.

We also found that the parameters α and β, which denote the decay and rise rate of the synaptic response, differentiate healthy sleep states from wake, and from brain-injured subjects. The characteristic duration of the synaptic response was found to be highest in normal non-REM sleep. We also showed that the threshold at $1/\alpha + 1/\beta \approx 30$ ms differentiated between subjects in NREM sleep, and those with severe brain injury. Conscious processing should be associated with

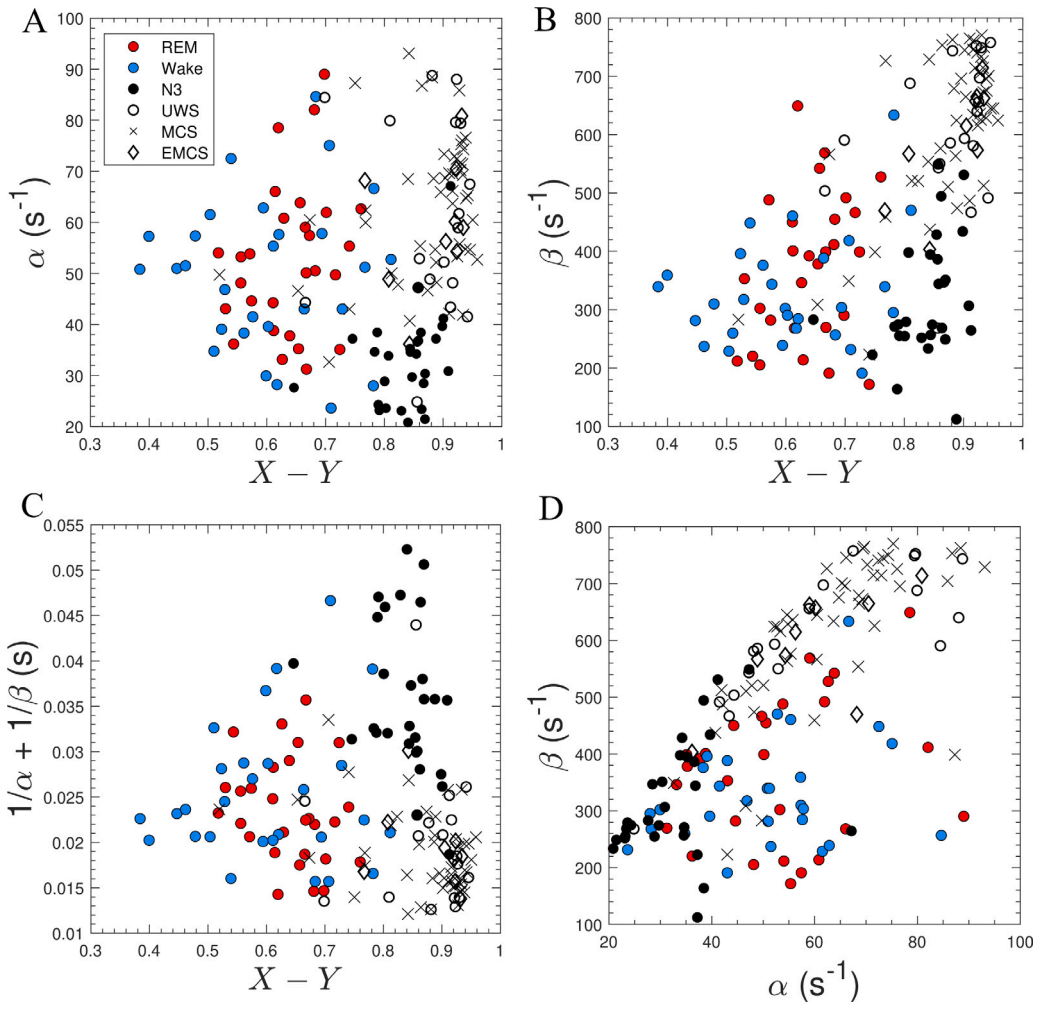

Fig. 8. Soma response rates vs. $X - Y$. (A) Individual averages of α and $X - Y$ during wake, REM, and deep sleep (N3), and for patients suffering from severe brain injury. The legend applies to all frames. (B) β vs. $X - Y$. (C) Effective duration of the soma response vs. $X - Y$. (D) β vs. α.

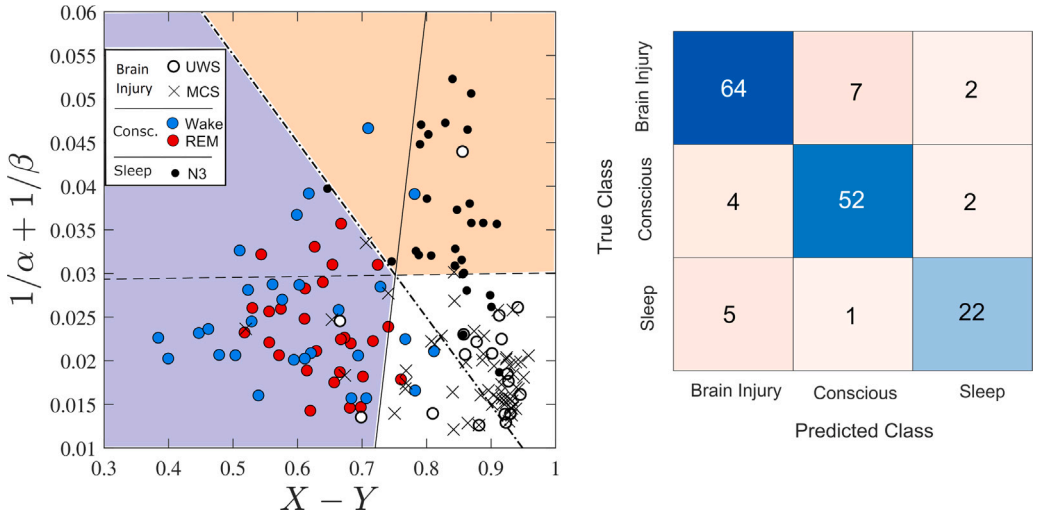

Fig. 9. LDA classification of subject groups. (A). Regions of healthy conscious, sleep, and brain injured patients. The solid line separates the conscious and brain-injured individuals. Subjects in normal sleep and brain-injured patients are separated by the dashed line. The dash-dot line separates healthy conscious and sleeping individuals. (B) Corresponding confusion matrix. The numbers along the rows and columns correspond to the true and predicted number of subjects in each class, respectively.

high frequency oscillations that respond fast, as a vehicle for conscious experiences (Hameroff, 2010), so longer synaptic latencies are likely to be associated to unconscious states or responses. Delayed synaptic responses have been proposed to be at the basis of altered consciousness

of several psychiatric diseases such as schizophrenia (Miterauer and Baer, 2020).

We emphasize that the method we use to extract physiological parameters, including the new measures of consciousness $X - Y$ and synaptic rates α and β, is computationally fast, such that the values can potentially be tracked in real time and at the bedside to give moment-by-moment estimates (unlike calculation of Φ from integrated information theory, for example, which is computationally prohibitive), e.g., to determine whether brief periods of greater consciousness are occurring. As shown previously, fluctuations of entropy in the EEG signals occur especially in MCS patients and might potentially depict moments of high and low consciousness (Piarulli et al., 2016). Indeed, also the behavioral assessments need to be repeated at least five times to reduce misdiagnosis, perhaps due to moments of low consciousness (Wannez et al., 2018). The method is also robust to noise and sudden changes in EEG (often due to artifacts that are prevalent in the EEG of patients with disorders of consciousness) because we use a Bayesian method to track temporal parameter changes. In this approach prior estimates of the fitted parameters are used to compute parameters during subsequent fits, thereby enforcing temporal continuity.

Overall, our method is able to distinguish between the three groupings of (i) wake and REM states, (ii) N3 sleep, and (iii) brain-injured states. However, resting state EEG does not appear to contain sufficient information with high enough signal to noise ratio to allow robust discrimination of the different brain-injured states (e.g., MCS vs. UWS) by fitting the parameters of the corticothalamic model. Several studies have suggested that basic measures such as delta and alpha band power or connectivity can be used for the diagnosis of disorder-of-consciousness (DoC) patients (Sitt et al., 2014); however, their use for the diagnosis of patients with a DoC could not be evaluated in a meta-analysis due to insufficient data (Kondziella et al., 2016). UK, US, and European guidelines only support the use of visual assessment of resting EEG data, mostly to rule out comorbidities such as epilepsy or hypertonus, which might confound behavioral evaluation (Giacino et al., 2018). A more recent systematic review qualitatively assesses that resting state EEG measures can be used for the diagnosis of patients with a DoC, but summarizing statistics are lacking (Bai et al., 2021).

Data acquired with a transcranial magnetic stimulation evoked-response protocol might be better suited to assess the capacity for conciousness (Casali et al., 2013). Lee and colleagues have used such evoked-response data to develop the explainable consciousness indicator, which can classify arousal and awareness levels in various pathological, pharmacological and pathological states of reduced consciousness (Lee et al., 2022). The corticothalamic model parameters can also be fitted to such evoked-response data, probably improving the fit as less noise is to be expected in such transcranial magnetic stimulation evoked responses. Nevertheless, the current work provides a proof of concept that EEG data acquired in brain-injured patients can be fitted via a corticothalamic model. Individual-subject trends in parameters over time may be more robust to track changes in the patients cerebral function than comparisons with group means. The thalamocortical model could in the future be fine-tuned for states of consciousness in patients with a DoC and provide a testing-ground for the evaluation of treatment on ongoing dynamics. The model could eventually be used for the identification of patients who might respond well to treatment, by the addition of plasticity parameters in the model. All these potential extensions and usages of the thalamocortical model will provide better understanding about the pathology of DoC and provide unique new avenues for the development of treatments in ways that are impossible with classical statistics or machine learning approaches.

Future studies could include further validation of our results against data from additional subjects. The results could also be extended to incorporate spatial information and to include measurements for additional groups of brain-injured subjects, including those suffering from locked-in syndrome, where conscious wakefulness is present despite the lack of voluntary movement, and also healthy individuals under different types of anesthesia. The effects of other structures could also be included; for example lesions in the basal forebrain would tend to reduce both X and Y parameters and are known to suppress wakefulness in rats (Fuller et al., 2011). Fits to stimulation data are also likely to be useful in distinguishing better between subtypes, as noted above.

CRediT authorship contribution statement

S. Assadzadeh: Writing – review & editing, Writing – original draft, Software, Methodology, Investigation, Formal analysis, Conceptualization. **J. Annen:** Writing – review & editing, Writing – original draft, Supervision, Methodology, Investigation, Data curation. **L. Sanz:** Methodology, Investigation, Data curation. **A. Barra:** Writing – review & editing, Methodology, Investigation, Data curation. **E. Bonin:** Writing – review & editing, Investigation, Data curation. **A. Thibaut:** Writing – review & editing, Investigation, Data curation. **M. Boly:** Writing – review & editing, Methodology, Investigation, Data curation. **S. Laureys:** Writing – review & editing, Supervision, Methodology, Investigation, Data curation. **O. Gosseries:** Writing – review & editing, Writing – original draft, Supervision, Methodology, Investigation, Data curation. **P.A. Robinson:** Writing – review & editing, Writing – original draft, Supervision, Methodology, Investigation, Conceptualization.

Declaration of competing interest

The authors have no competing interests to declare.

Data availability

Data will be made available on request.

Acknowledgments

We thank D. Naoumenko for assistance with Figs. 4–6. This work was supported by the Australian Research Council Center of Excellence for Integrative Brain Function under ARC grant CE140100007, the Australian Research Council Laureate Fellowship Grant FL140100025. The study was further supported by the University and University Hospital of Liege, the Belgian National Funds for Scientific Research (FRS-FNRS), the European Union's Horizon 2020 Framework Programme for Research and Innovation under the Specific Grant Agreement No. 945539 (Human Brain Project SGA3), the European Space Agency (ESA), France and the Belgian Federal Science Policy Office (BELSPO) in the framework of the PRODEX Programme, "Fondazione Europea di Ricerca Biomedica", the BIAL Foundation, the Mind Science Foundation, USA and the European Commission, the fund Generet, the Mind Care International Foundation, the King Baudouin Foundation, USA, DOCMA project [EU-H2020-MSCA–RISE–778234]. OG is research associate and SL is research director at the FNRS. We are highly grateful to the members of the Liège Coma Science Group for their assistance in clinical evaluations. We would also like to thank R. G. Abeysuriya for providing parameters belonging to the sleep stages used in this study.

Ethics statement

All the experimental procedures were approved by the ethical committee at the Medicine Faculty of the University of Liege, Belgium. All healthy participants gave written informed consent, while for non-communicating brain-injured patients the informed consent was obtained from a legal surrogate.

References

Abeysuriya, R.G., Rennie, C.J., Robinson, P.A., 2015. Physiologically based arousal state estimation and dynamics. J. Neurosci. Methods 253, 55–69. http://dx.doi.org/10.1016/j.jneumeth.2015.06.002.

Abeysuriya, R.G., Robinson, P.A., 2016. Real-time automated EEG tracking of brain states using neural field theory. J. Neurosci. Methods 258, 28–45. http://dx.doi.org/10.1016/j.jneumeth.2015.09.026.

Assadzadeh, S., Robinson, P.A., 2018. Necessity of the sleep–wake cycle for synaptic homeostasis: system-level analysis of plasticity in the corticothalamic system. R. Soc. Open Sci. 5 (10), 171952. http://dx.doi.org/10.1098/rsos.171952.

Baars, B.J., 2002. The conscious access hypothesis: Origins and recent evidence. Trends in Cognitive Sciences 6 (1), 47–52. http://dx.doi.org/10.1016/S1364-6613(00)01819-2.

Bai, Y., Lin, Y., Ziemann, U., 2021. Managing disorders of consciousness: The role of electroencephalography. J. Neurol. 268, 4033–4065.

Bodart, O., Gosseries, O., Wannez, S., Thibaut, A., Annen, J., Boly, M., et al., 2017. Measures of metabolism and complexity in the brain of patients with disorders of consciousness. NeuroImage: Clinical 14, 354–362.

Boveroux, P., Vanhaudenhuyse, A., Bruno, M.-A., Noirhomme, Q., Lauwick, S., Luxen, A., et al., 2010. Breakdown of within-and between-network resting state functional magnetic resonance imaging connectivity during propofol-induced loss of consciousness. Anesthesiology: J. Am. Soc. Anesthesiol. 113 (5), 1038–1053.

Braitenberg, V., Schüz, A., 1998. Cortex: Statistics and Geometry of Neuronal Connectivity. Springer-Verlag, Berlin Heidelberg.

Breakspear, M., Roberts, J.A., Terry, J.R., Rodrigues, S., Mahant, N., Robinson, P.A., 2006. A unifying explanation of primary generalized seizures through nonlinear brain modeling and bifurcation analysis. Cereb Cortex 16 (9), 1296–1313. http://dx.doi.org/10.1093/cercor/bhj072.

Bruno, M.-A., Vanhaudenhuyse, A., Thibaut, A., Moonen, G., Laureys, S., 2011. From unresponsive wakefulness to minimally conscious PLUS and functional locked-in syndromes: recent advances in our understanding of disorders of consciousness. J. Neurol. 258 (7), 1373–1384. http://dx.doi.org/10.1007/s00415-011-6114-x.

Casali, A.G., Gosseries, O., Rosanova, M., Boly, M., Sarasso, S., Casali, K.R., et al., 2013. A theoretically based index of consciousness independent of sensory processing and behavior. Sci. Transl. Med. 5 (198), 198ra105. http://dx.doi.org/10.1126/scitranslmed.3006294.

Casarotto, S., Comanducci, A., Rosanova, M., Sarasso, S., Fecchio, M., Napolitani, M., et al., 2016. Stratification of unresponsive patients by an independently validated index of brain complexity. Annals of Neurology 80 (5), 718–729.

Deco, G., Jirsa, V.K., Robinson, P.A., Breakspear, M., Friston, K., 2008. The dynamic brain: From spiking neurons to neural masses and cortical fields. PLoS Comput. Biol. 4 (8), e1000092. http://dx.doi.org/10.1371/journal.pcbi.1000092.

Dehaene, S., Sergent, C., Changeux, J.-P., 2003. A neuronal network model linking subjective reports and objective physiological data during conscious perception. Proc. Nat. Acad. Sci. USA 100 (14), 8520–8525. http://dx.doi.org/10.1073/pnas.1332574100.

D'Rozario, A.L., Kim, J.W., Wong, K.K.H., Bartlett, D.J., Marshall, N.S., Dijk, D.-J., et al., 2013. A new EEG biomarker of neurobehavioural impairment and sleepiness in sleep apnea patients and controls during extended wakefulness. Clin. Neurophysiol. 124 (8), 1605–1614. http://dx.doi.org/10.1016/j.clinph.2013.02.022.

Edelman, G.M., 2003. Naturalizing consciousness: A theoretical framework. Proc. Natl. Acad. Sci. USA 100 (9), 5520–5524. http://dx.doi.org/10.1073/pnas.0931349100.

Fernández-Espejo, D., Rossit, S., Owen, A.M., 2015. A thalamocortical mechanism for the absence of overt motor behavior in covertly aware patients. JAMA Neurol. 72 (12), 1442–1450.

Freeman, W.J., 1975. Mass Action in the Nervous System: Examination of the Neurophysiological Basis of Adaptive Behavior Through the EEG. Academic Press, New York.

Freeman, W.J., 2007. Indirect biological measures of consciousness from field studies of brains as dynamical systems. Brain and consciousness, Neural Netw. Brain and consciousness, 20 (9), 1021–1031.http://dx.doi.org/10.1016/j.neunet.2007.09.004,

Fuller, P., Sherman, D., Pedersen, N., Saper, C., Lu, J., 2011. Reassessment of the structural basis of the ascending arousal system. J Compar. Neurol. 519, 933–956.

Gan, T.J., Glass, P.S., Windsor, A., Payne, F., Rosow, C., Sebel, P., et al., 1997. Bispectral index monitoring allows faster emergence and improved recovery from propofol, alfentanil, and nitrous oxide anesthesia. Anesthes 87 (4), 808–815.

Giacino, J.T., Kalmar, K., Whyte, J., 2004. The JFK coma recovery scale – revised: Measurement characteristics and diagnostic utility. Arch. Phys. Med. Rehabil. 85 (12), 2020–2029.

Giacino, J.T., et al., 2018. Practice guideline update recommendations summary: Disorders of consciousness: Report of the guideline development, dissemination, and implementation subcommittee of the American academy of neurology; the American congress of rehabilitation medicine; and the national institute on disability, independent living, and rehabilitation research. Neurology 91, 450–460.

Gosseries, O., Bruno, M.-A., Chatelle, C., Vanhaudenhuyse, A., Schnakers, C., Soddu, A., et al., 2011a. Disorders of consciousness: what's in a name? NeuroRehabilitation 28 (1), 3–14.

Gosseries, O., Schnakers, C., Ledoux, D., Vanhaudenhuyse, A., Bruno, M.-A., Demertzi, A., et al., 2011b. Automated EEG entropy measurements in coma, vegetative state/unresponsive wakefulness syndrome and minimally conscious state. Funct. Neurol. 26 (1), 25–30.

Guldenmund, P., Vanhaudenhuyse, A., Sanders, R., Sleigh, J., Bruno, M.-A., Demertzi, A., et al., 2017. Brain functional connectivity differentiates dexmedetomidine from propofol and natural sleep. BJA: Br. J. Anaesthesia 119 (4), 674–684.

Hameroff, S., 2010. The "conscious pilot"—dendritic synchrony moves through the brain to mediate consciousness. J. Biol. Phys. 36 (1), 71–93.

Hastings, W.K., 1970. Monte Carlo sampling methods using Markov chains and their applications. Biometrika 57 (1), 97–109. http://dx.doi.org/10.1093/biomet/57.1.97.

Jirsa, V.K., Haken, H., 1996. Field theory of electromagnetic brain activity. Phys. Rev. Lett. 77, 960–963.

Kerr, C.C., Rennie, C.J., Robinson, P.A., 2008. Physiology-based modeling of cortical auditory evoked potentials. Biol. Cybern. 98 (2), 171–184. http://dx.doi.org/10.1007/s00422-007-0201-1.

Kim, H., Hudetz, A.G., Lee, J., Mashour, G.A., Lee, U., Group the ReCCognition Study, et al., 2018. Estimating the integrated information measure Phi from high-density electroencephalography during states of consciousness in humans. Front. Hum. Neurosci. 12, http://dx.doi.org/10.3389/fnhum.2018.00042.

Kim, K.H., Relkin, N.R., Lee, K.-M., Hirsch, J., 1997. Distinct cortical areas associated with native and second languages. Nature 388 (6638), 171–174.

Koch, C., Massimini, M., Boly, M., Tononi, G., 2016. Neural correlates of consciousness: progress and problems. Nat. Rev. Neurosci. 17 (5), 22. http://dx.doi.org/10.1038/nrn.2016.22.

Kondziella, D., Friberg, C.K., Frokjaer, V.G., Fabricius, M., Møller, 2016. Preserved consciousness in vegetative and minimal consciousness states: Systematic review and meta-analysis. J. Neurol. Neurosurg. Psychiatry 87, 485–492.

Laureys, S., Boly, M., Moonen, G., Maquet, P., 2009. Two dimensions of consciousness: Arousal and awareness. Encycl. Neurosci. 2, 1133–1142.

Laureys, S., Celesia, G.G., Cohadon, F., Lavrijsen, J., León-Carrión, J., Sannita, W.G., et al., 2010. Unresponsive wakefulness syndrome: a new name for the vegetative state or apallic syndrome. BMC Medi. 8 (1), 1–4.

Laureys, S., Owen, A.M., Schiff, N.D., 2004. Brain function in coma, vegetative state, and related disorders. Lancet Neurol. 3 (9), 537–546. http://dx.doi.org/10.1016/S1474-4422(04)00852-X.

Laureys, S., Schiff, N.D., 2012. Coma and consciousness: Paradigms (re)framed by neuroimaging. NeuroImage 61 (2), 478–491. http://dx.doi.org/10.1016/j.neuroimage.2011.12.041.

Lee, M., et al., 2022. Quantifying arousal and awareness in altered states of consciousness using interpretable deep learning. Nat. Commun. 13, 1064.

Lopes da Silva, F.H., Hoeks, A., Smits, H., Zetterberg, L.H., 1974. Model of brain rhythmic activity. Kybernetik 15 (1), 27–37. http://dx.doi.org/10.1007/BF00270757.

Mashour, G.A., Shanks, A., Tremper, K.K., Kheterpal, S., Turner, C.R., Ramachandran, S.K., et al., 2012. Prevention of intraoperative awareness with explicit recall in an unselected surgical population: A randomized comparative effectiveness trial. Anesthes 117 (4), 717–725. http://dx.doi.org/10.1097/ALN.0b013e31826904a6.

MATLAB, 2019. version 9.7.0.1216025 (R2019b). The MathWorks Inc., Natick, Massachusetts.

Metropolis, N., Rosenbluth, A.W., Rosenbluth, M.N., Teller, A.H., Teller, E., 1953. Equation of state calculations by fast computing machines. J. Chem. Phys. 21 (6), 1087–1092.

Metzinger, T., 1995. Conscious Experience. Imprint Academic, Schöningh.

Metzinger, T., 2000. Neural Correlates of Consciousness: Empirical and Conceptual Questions. MIT Press, Cambridge, MA.

Min, B.-K., Kim, H.S., Pinotsis, D.A., Pantazis, D., 2020. Thalamocortical inhibitory dynamics support conscious perception. NeuroImage 220, 117066.

Miterauer, B., Baer, W., 2020. Disorders of human consciousness in the tri-partite synapses. Med. Hypotheses 136, 109523.

Monti, M.M., Rosenberg, M., Finoia, P., Kamau, E., Pickard, J.D., Owen, A.M., 2015. Thalamo-frontal connectivity mediates top-down cognitive functions in disorders of consciousness. Neurology 84 (2), 167–173.

Müller, E.J., van Albada, S.J., Kim, J.W., Robinson, P.A., 2017. Unified neural field theory of brain dynamics underlying oscillations in Parkinson's disease and generalized epilepsies. J. Theoret. Biol. 428, 132–146. http://dx.doi.org/10.1016/j.jtbi.2017.06.016.

Myles, P., Leslie, K., McNeil, J., Forbes, A., Chan, M., 2004. Bispectral index monitoring to prevent awareness during anaesthesia: the B-Aware randomised controlled trial. Lancet 363 (9423), 1757–1763. http://dx.doi.org/10.1016/S0140-6736(04)16300-9.

Niedermeyer, E., Lopes da Silva, F.H., 2005. Electroencephalography: Basic Principles, Clinical Applications, and Related Fields. Lippincott Williams & Wilkins, Philadelphia.

Nunez, P.L., Srinivasan, R., 2006. Electric Fields of the Brain: the Neurophysics of EEG. Oxford University Press, New York.

O'Connor, S.C., Robinson, P.A., 2004. Spatially uniform and nonuniform analyses of electroencephalographic dynamics, with application to the topography of the alpha rhythm. Phys. Rev. E 70 (1), 011911. http://dx.doi.org/10.1103/PhysRevE.70.011911.

Oizumi, M., Albantakis, L., Tononi, G., 2014. From the phenomenology to the mechanisms of consciousness: Integrated information theory 3.0. PLoS Comput. Biol. 10 (5), 1–25. http://dx.doi.org/10.1371/journal.pcbi.1003588.

Piarulli, A., Bergamasco, M., Thibaut, A., Cologan, V., Gosseries, O., Laureys, S., 2016. EEG ultradian rhythmicity differences in disorders of consciousness during wakefulness. J. Neurol. 263 (9), 1746–1760.

Rennie, C.J., Robinson, P.A., Wright, J.J., 2002. Unified neurophysical model of EEG spectra and evoked potentials. Biol. Cybern. 86 (6), 457–471. http://dx.doi.org/10.1007/s00422-002-0310-9.

Revonsuo, A., Newman, J.B., 1999. Binding and consciousness. Conscious. Cogn. 8 (2), 123–127.

Roberts, J.A., Robinson, P.A., 2012. Corticothalamic dynamics: Structure of parameter space, spectra, instabilities, and reduced model. Phys. Rev. E 85 (1), 011910. http://dx.doi.org/10.1103/PhysRevE.85.011910.

Robinson, P.A., 2003. Neurophysical theory of coherence and correlations of electroencephalographic and electrocorticographic signals. J. Theoret. Biol. 222 (2), 163–175. http://dx.doi.org/10.1016/S0022-5193(03)00023-7.

Robinson, P.A., 2005. Propagator theory of brain dynamics. Phys. Rev. E 72 (1), 011904. http://dx.doi.org/10.1103/PhysRevE.72.011904.

Robinson, P.A., 2011. Neural field theory of synaptic plasticity. J. Theoret. Biol. 285 (1), 156–163. http://dx.doi.org/10.1016/j.jtbi.2011.06.023.

Robinson, P.A., 2017. The balanced and introspective brain. J. R. Soc. Interface 14 (130), 20160994. http://dx.doi.org/10.1098/rsif.2016.0994, URL http://rsif.royalsocietypublishing.org/content/14/130/20160994.

Robinson, P.A., Loxley, P.N., O'Connor, S.C., Rennie, C.J., 2001. Modal analysis of corticothalamic dynamics, electroencephalographic spectra, and evoked potentials. Phys. Rev. E 63 (4 Pt 1), 041909. http://dx.doi.org/10.1103/PhysRevE.63.041909.

Robinson, P.A., Rennie, C.J., Rowe, D.L., 2002. Dynamics of large-scale brain activity in normal arousal states and epileptic seizures. Phys. Rev. E 65 (4), 041924. http://dx.doi.org/10.1103/PhysRevE.65.041924.

Robinson, P.A., Rennie, C.J., Rowe, D.L., O'Connor, S.C., 2004. Estimation of multiscale neurophysiologic parameters by electroencephalographic means. Hum. Brain Mapp. 23 (1), 53–72. http://dx.doi.org/10.1002/hbm.20032.

Robinson, P.A., Rennie, C.J., Wright, J.J., Bourke, P.D., 1998. Steady states and global dynamics of electrical activity in the cerebral cortex. Phys. Rev. E 58 (3), 3557–3571. http://dx.doi.org/10.1103/PhysRevE.58.3557.

Rosanova, M., Fecchio, M., Casarotto, S., Sarasso, S., Casali, A., Pigorini, A., et al., 2018. Sleep-like cortical OFF-periods disrupt causality and complexity in the brain of unresponsive wakefulness syndrome patients. Nature Commun. 9 (1), 1–10.

Rowe, D.L., Robinson, P.A., Rennie, C.J., 2004. Estimation of neurophysiological parameters from the waking EEG using a biophysical model of brain dynamics. J. Theoret. Biol. 231 (3), 413–433. http://dx.doi.org/10.1016/j.jtbi.2004.07.004.

Sanders, R.D., Tononi, G., Laureys, S., Sleigh, J., 2012. Unresponsiveness ≠ Unconsciousness. Anesthesiology 116 (4), 946–959. http://dx.doi.org/10.1097/ALN.0b013e318249d0a7.

Schmidt, T.T., Jagannathan, N., Ljubljanac, M., Xavier, A., Nierhaus, T., 2020. The multimodal ganzfeld-induced altered state of consciousness induces decreased thalamo-cortical coupling. Sci. Rep. 10 (1), 1–10.

Seth, A.K., Dienes, Z., Cleeremans, A., Overgaard, M., Pessoa, L., 2008. Measuring consciousness: Relating behavioural and neurophysiological approaches. Trends Cogn. Sci. 12 (8), 314–321. http://dx.doi.org/10.1016/j.tics.2008.04.008.

Seth, A.K., Izhikevich, E., Reeke, G.N., Edelman, G.M., 2006. Theories and measures of consciousness: An extended framework. Proc. Nat. Acad. Sci. USA 103 (28), 10799–10804. http://dx.doi.org/10.1073/pnas.0604347103.

Sitt, J.D., et al., 2014. Large scale screening of neural signatures of consciousness in patients in a vegetative or minimally conscious state. Brain 137, 2258–2270.

Srinivasan, R., Nunez, P.L., Silberstein, R.B., 1998. Spatial filtering and neocortical dynamics: Estimates of EEG coherence. IEEE Trans. Biomed. Eng. 45 (7), 814–826.

Stam, C.J., 2005. Nonlinear dynamical analysis of EEG and MEG: Review of an emerging field. Clin. Neurophysiol. 116 (10), 2266–2301.

Suffczynski, P., Kalitzin, S., Pfurtscheller, G., Lopes Da Silva, F.H., 2001. Computational model of thalamo-cortical networks: dynamical control of alpha rhythms in relation to focal attention. Int. J. Psychophysiol. 43 (1), 25–40.

Tononi, G., 2008. Consciousness as integrated information: A provisional manifesto. Biol. Bull. 215 (3), 216–242. http://dx.doi.org/10.2307/25470707.

Tononi, G., 2012. Integrated information theory of consciousness: An updated account. Arch. Ital. Biol. 150 (2–3), 56–90. http://dx.doi.org/10.4449/aib.v149i5.1388.

Tononi, G., Boly, M., Massimini, M., Koch, C., 2016. Integrated information theory: From consciousness to its physical substrate. Nat. Rev. Neurosci. 17 (7), 450–461. http://dx.doi.org/10.1038/nrn.2016.44.

van Albada, S.J., Kerr, C.C., Chiang, A.K.I., Rennie, C.J., Robinson, P.A., 2010. Neurophysiological changes with age probed by inverse modeling of EEG spectra. Clin. Neurophysiol. 121 (1), 21–38. http://dx.doi.org/10.1016/j.clinph.2009.09.021.

van Albada, S.J., Robinson, P.A., 2009. Mean-field modeling of the basal ganglia-thalamocortical system. I: Firing rates in healthy and parkinsonian states. J. Theoret. Biol. 257 (4), 642–663. http://dx.doi.org/10.1016/j.jtbi.2008.12.018.

Wang, D., Teichtahl, H., Drummer, O., Goodman, C., Cherry, G., Cunnington, D., et al., 2005. Central sleep apnea in stable methadone maintenance treatment patients. Chest 128 (3), 1348–1356. http://dx.doi.org/10.1378/chest.128.3.1348.

Wannez, S., Gosseries, O., Azzolini, D., Martial, C., Cassol, H., Aubinet, C., et al., 2018. Prevalence of coma-recovery scale-revised signs of consciousness in patients in minimally conscious state. Neuropsychol. Rehabil. 28 (8), 1350–1359.

Wright, J.J., Liley, D.T.J., 1996. Dynamics of the brain at global and microscopic scales: Neural networks and the EEG. Behav. Brain Sci. 19 (2), 285.

Zhao, X., Robinson, P.A., 2015. Generalized seizures in a neural field model with bursting dynamics. J. Comput. Neurosci. 39 (2), 197–216. http://dx.doi.org/10.1007/s10827-015-0571-7.

Zobaer, M.S., Robinson, P.A., Kerr, C.C., 2018. Physiology-based ERPs in normal and abnormal states. Biol. Cybern. 112 (5), 465–482. http://dx.doi.org/10.1007/s00422-018-0766-x.